Immunological memory to SARS-CoV-2 assessed for greater than six months after infection

Jennifer M. Dan[1,3]*, Jose Mateus[1]*, Yu Kato[1]*, Kathryn M. Hastie[1], Caterina E. Faliti[1], Sydney I. Ramirez[1,3], April Frazier[1], Esther Dawen Yu[1], Alba Grifoni[1], Stephen A. Rawlings[3], Bjoern Peters[1,2], Florian Krammer[4], Viviana Simon[4,5,6], Erica Ollmann Saphire[1,3], Davey M. Smith[3], Daniela Weiskopf[1]^, Alessandro Sette[1,3]^, Shane Crotty[1,3]^

[1] Center for Infectious Disease and Vaccine Research, La Jolla Institute for Immunology (LJI), La Jolla, CA 92037, USA
[2] Department of Medicine, University of California, San Diego (UCSD), La Jolla, CA 92037, USA
[3] Department of Medicine, Division of Infectious Diseases and Global Public Health, University of California, San Diego (UCSD), La Jolla, CA 92037, USA
[4] Department of Microbiology, Icahn School of Medicine at Mount Sinai, New York, New York
[5] Division of Infectious Diseases, Department of Medicine, Icahn School of Medicine at Mount Sinai, New York, NY 10029, USA
[6] The Global Health and Emerging Pathogens Institute, Icahn School of Medicine at Mount Sinai, New York, NY 10029, USA

* These authors contributed equally
^ Correspondence: shane@lji.org (S.C.), alex@lji.org (A.S.), daniela@lji.org (D.W.)

ABSTRACT

Understanding immune memory to SARS-CoV-2 is critical for improving diagnostics and vaccines, and for assessing the likely future course of the pandemic. We analyzed multiple compartments of circulating immune memory to SARS-CoV-2 in 185 COVID-19 cases, including 41 cases at $\geq$ 6 months post-infection. Spike IgG was relatively stable over 6+ months. Spike-specific memory B cells were more abundant at 6 months than at 1 month. SARS-CoV-2-specific $CD4^+$ T cells and $CD8^+$ T cells declined with a half-life of 3-5 months. By studying antibody, memory B cell, $CD4^+$ T cell, and $CD8^+$ T cell memory to SARS-CoV-2 in an integrated manner, we observed that each component of SARS-CoV-2 immune memory exhibited distinct kinetics.

INTRODUCTION

Coronavirus disease 2019 (COVID-19), caused by the novel severe acute respiratory syndrome coronavirus 2 (SARS-CoV-2), is a serious disease that has resulted in widespread global morbidity and mortality. Humans make SARS-CoV-2-specific antibodies, $CD4^+$ T cells, and $CD8^+$ T cells in response to SARS-CoV-2 infection (*1–4*). Studies of acute and convalescent COVID-19 patients have observed that T cell responses are associated with lessened disease (*5–7*), suggesting that SARS-CoV-2-specific $CD4^+$ T cell and $CD8^+$ T cell responses may be important for control and resolution of primary SARS-CoV-2 infection. Ineffective innate immunity has been strongly associated with a lack of control of primary SARS-CoV-2 infection and a high risk of fatal COVID-19 (*8–12*), accompanied by innate cell immunopathology (*13–18*). Neutralizing antibodies have generally not correlated with lessened COVID-19 disease severity (*5*, *19*, *20*), which was also observed for Middle Eastern respiratory syndrome (MERS), caused by infection with the human coronavirus MERS-CoV (*21*). Instead, neutralizing antibodies are associated with protective immunity against secondary (2°) infection with SARS-CoV-2 or SARS-CoV in non-human primates (*3*, *22–25*). Additionally, human subjects with detectable neutralizing antibodies were protected from 2° COVID-19 in a ship outbreak (*26*). Passive transfer of neutralizing antibodies in advance of infection (mimicking the conditions of 2° infection) effectively limits upper respiratory tract (URT) infection, lower respiratory tract (lung) infection, and symptomatic disease in animal models (*27–29*). Passive transfer of neutralizing antibodies provided after initiation of infection in humans have had more limited effects on COVID-19 (*30*, *31*), consistent with a substantial role for T cells in control and clearance of an ongoing SARS-CoV-2 infection. Thus, studying antibody, memory B cell, $CD4^+$ T cell, and $CD8^+$ T cell memory to SARS-CoV-2 in an integrated manner is likely important for understanding the durability of protective immunity against COVID-19 generated by primary SARS-CoV-2 infection (*1*, *19*, *32*).

While sterilizing immunity against viruses can only be accomplished by high-titer neutralizing antibodies, successful protection against clinical disease or death can be accomplished by several other adaptive immune memory scenarios. Possible mechanisms of immunological protection can vary based on the relative kinetics of the immune memory responses and infection. For example, clinical hepatitis after hepatitis B virus (HBV) infection is prevented by vaccine-elicited immune memory even in the absence of circulating antibodies, because of the relatively slow course of HBV disease (*33*, *34*). The relatively slow course of severe COVID-19 in humans (median 19 days post-symptom onset (PSO) for fatal cases (*35*)) suggests that protective immunity against symptomatic or severe 2° COVID-19 may very well involve memory compartments such as circulating memory T cells and memory B cells (which can take several days to reactivate and generate recall T cell responses and/or anamnestic antibody responses) (*19*, *21*, *32*).

Immune memory, from either primary infection or immunization, is the source of protective immunity from a subsequent infection (*36–38*). Thus, COVID-19 vaccine development is closely tied to the topic of immunological memory (*1*, *3*). Despite intensive study, the kinetics, duration, and evolution of immune memory in humans to infection or immunization are not in general predictable based on the initial effector phase, and immune responses at short time points after resolution of infection are not very predictive of long-term memory (*39–41*). Thus, assessing responses over an interval of six months or more is usually required to ascertain the durability of immune memory.

A thorough understanding of immune memory to SARS-CoV-2 requires evaluation of its various components, including B cells, $CD8^+$ T cells, and $CD4^+$ T cells, as these different cell types may have immune memory kinetics relatively independent of each other. Understanding the complexities of immune memory to SARS-CoV-2 is key to gain insights into the likelihood of durability of protective immunity against re-infection with SARS-CoV-2 and 2° COVID-19 disease. In the current study, we assessed immune memory of all three branches of adaptive immunity ($CD4^+$ T cell, $CD8^+$ T cell, and

humoral immunity) in a cross-sectional study of 185 recovered COVID-19 cases, extending out to greater than six months post-infection. The findings have implications for immunity against 2° COVID-19, and thus the potential future course of the pandemic (*42*, *43*).

COVID-19 cohort

185 individuals with COVID-19 were recruited for this study. Subjects (43% male, 57% female) represented a range of asymptomatic, mild, moderate, and severe COVID-19 cases (Table S1), and were recruited from multiple sites throughout the United States. The majority of subjects were from California or New York. The majority of subjects had a mild case of COVID-19, not requiring hospitalization. 92% of subjects were never hospitalized for COVID-19; 7% of subjects were hospitalized, some of whom required intensive care unit (ICU) care (Table S1; hospitalization requirement not reported for 1 subject), consistent with the COVID-19 disease severity distribution in the USA. The majority of subjects (97%) reported symptomatic disease (Table S1; not reported for 1 subject). The ages of the subjects ranged from 19 to 81 years old (Table S1). Most subjects provided a blood sample at a single time point, between 6 days (d) post-symptom onset (PSO) and 240d PSO (Table S1), with 41 samples at $\geq$ six months PSO (d178 or longer). Thirty-eight subjects provided longitudinal blood samples over a duration of several months (2-4 time points. Table S1).

SARS-CoV-2 circulating antibodies over time

The vast majority of SARS-CoV-2 infected individuals seroconvert, at least for a duration of months (*1*, *2*, *4*, *20*, *44–46*). These estimates range from 91-99% in large studies (*20*, *46*). Durability assessments of circulating antibody titers in Figure 1 were based on data $\geq$ 20d PSO, using curve fits modeling a continuous decay, one-phased decay, or two-phased decay, with the best fitting model shown in blue. Negative and positive controls were used to standardize each assay and normalize across experiments. SARS-CoV-2 spike IgG endpoint ELISA titers in plasma were measured for all subjects of this cohort (**Fig. 1A-B**). Spike receptor binding domain (RBD) IgG was also measured (**Fig. 1C-D**), as RBD is the target of the vast majority of neutralizing antibodies against SARS-CoV-2 (*4*, *28*, *47*, *48*). SARS-CoV-2 pseudovirus (PSV) neutralizing antibody titers were measured in all subjects, as the functional complement of the antibody binding assays (**Fig. 1E-F**). Nucleocapsid (N) IgG endpoint ELISA titers were also measured for all subjects (**Fig. 1G-H**), as nucleocapsid is a common antigen in commercial SARS-CoV-2 serological test kits.

SARS-CoV-2 spike IgG titers were nearly stable from d20-d240 PSO, when assessing all COVID-19 subjects by cross-sectional analysis (half-life $t_{1/2}$ = 140d, **Fig. 1A**). Spike IgG titers were heterogenous among subjects (range 5 to 73,071; 575 median), as has been widely observed (*20*, *48*). This gave a wide confidence interval for the spike IgG $t_{1/2}$ (95% CI: 89 to 329d). While the antibody responses likely have underlying bi-phasic decay kinetics, the best fit curve was a linear decay, probably related to heterogeneity between individuals. SARS-CoV-2 nucleocapsid IgG kinetics were similar to spike IgG over 8 months ($t_{1/2}$ 67d, 95% CI: 49-105d. **Fig. 1G**). As a complementary approach, using paired samples from the subset of subjects who donated at two or more time points, the calculated spike IgG titer average $t_{1/2}$ was 100d, (95% CI: 64-220d, **Fig. 1B**) and the nucleocapsid IgG titer average $t_{1/2}$ was 67d, (95% CI: 54-88d, **Fig. 1H**). The percentage of subjects seropositive for spike IgG at 1 month PSO (d20-50) was 98% (54/55). The percentage of subjects seropositive for spike IgG at 6 to 8 months PSO (d >178) was 90% (36/40).

Cross-sectional analysis SARS-CoV-2 RBD IgG titers from d20-d240 PSO gave an estimated $t_{1/2}$ of 83d, 95% CI 62-127d (**Fig. 1C**). As a complementary approach, we again used paired samples, which gave an average $t_{1/2}$ of 68d, 95% CI: 57-85d (**Fig. 1D**). The percentage of subjects seropositive for RBD IgG at 6 to 8 months PSO was 88% (35/40). Thus, the RBD IgG titer maintenance largely matched that of

spike IgG. SARS-CoV-2 PSV neutralization titers in the full cohort largely matched the results of SARS-CoV-2 RBD IgG ELISA binding titers (**Fig.1E-F**). A one-phase decay model was the best fit (P=0.015, F test. Initial decay $t_{1/2}$ 27d, followed by an extended plateau phase. **Fig. 1E**), while a linear decay gave an estimated $t_{1/2}$ of 114d. Paired timepoints analysis of the PSV neutralization titers gave an estimated $t_{1/2}$ 87d, (95% CI: 68-123d, **Fig. 1F**). The percentage of subjects seropositive for SARS-CoV-2 neutralizing antibodies (titer $\geq$ 20) at 6 to 8 months PSO was 90% (36/40). Notably, even low levels of circulating neutralizing antibody titers ($\geq$ 1:20) were associated with a substantial degree of protection against COVID-19 in non-human primates (*24*, *49*). Thus, modest levels of circulating SARS-CoV-2 neutralizing antibodies are of biological interest in humans.

SARS-CoV-2 spike IgA (**Fig. 1I-J**) and RBD IgA (**Fig.1K-L**) titers were also assessed. Paired timepoints analysis of spike IgA titers yielded an estimated $t_{1/2}$ of 214d, 95% CI 126-703d (**Fig. 1J**). Cross-sectional analysis of spike IgA fit a shohrt one-phase decay model with an extended plateau phase (initial $t_{1/2}$ of 11d, **Fig. 1I**). Circulating RBD IgA had an estimated $t_{1/2}$ of 27d, 95% CI 15-58d, decaying by ~90d in a majority of COVID-19 cases to levels indistinguishable from uninfected controls (**Fig. 1K**), consistent with observations 3 months PSO (*46*, *50*). By paired sample analysis, long-lasting RBD IgA was made in some subjects, but often near the limit of sensitivity (LOS) (**Fig. 1L**).

SARS-CoV-2 memory B cells

To identify SARS-CoV-2-specific memory B cells, fluorescently labeled multimerized probes were used to detect B cells specific to spike, RBD, and nucleocapsid (**Fig 2A,** Fig. S1). Antigen-binding memory B cells (defined as IgD^- and/or $CD27^+$) were further distinguished according to surface immunoglobulin (Ig) isotypes: IgM, IgG or IgA (**Fig. 2B,** Fig. S1).

Spike-specific memory B cells in SARS-CoV-2 unexposed donors were rare (median 0.0078%. **Fig 2A, 2C.**). Cross-sectional analysis revealed that frequencies of SARS-CoV-2 spike-specific memory B cells increased over the first ~150d PSO and then plateaued (Pseudo-first order model for best fit curve. R^2 = 0.14. Better fit than second order polynomial model by Akaike's Information Criterion. **Fig 2C,** Fig. S2A). Spike-specific memory B cell frequencies increased from the first time-point (d36-d163) to the second time-point (d111-d240) in paired samples from 24 of 36 longitudinally tracked donors (**Fig 2D**).

RBD-specific memory B cells displayed similar kinetics to spike-specific memory B cells. As expected, RBD-specific memory B cells were undetectable in SARS-CoV-2 unexposed subjects (**Fig. 2E.** Fig. S2C). RBD-specific memory B cells appeared as early as 16d PSO, and the frequency steadily increased in the following 4-5 months (**Fig. 2E.** Fig. S2B-C). 29 of 36 longitudinally tracked individuals had higher frequencies of RBD-specific memory B cells at the later time point (**Fig. 2F**), again showing an increase in SARS-CoV-2 specific memory B cells several months post-infection. ~10-30% of spike-specific memory B cells from SARS-CoV-2 convalescent donors were specific for the RBD domain (**Fig. 2A,** Fig. S2B).

SARS-CoV-2 nucleocapsid-specific memory B cells were also detected after SARS-CoV-2 infection (**Fig. 2A**). Similar to spike- and RBD-specific memory B cells, nucleocapsid-specific memory B cell frequency steadily increased during the first ~5 months PSO (**Fig. 2G, 2H,** Fig. S2D). Antibody affinity maturation could potentially explain the increased frequencies of SARS-CoV-2-specific memory B cells detected by the antigen probes. However, geometric mean fluorescent intensity (MFI) of probe binding was stable over time (Fig. S2I-J), not supporting an affinity maturation explanation for the increased memory B cell frequencies.

Representation of Ig isotypes among the SARS-CoV-2 spike-specific memory B cell population shifted with time (**Fig. 2I-2O**). During the earliest phase of memory (20-60d PSO), IgM^+ and IgG^+ isotypes were similarly represented (**Fig. 2O**), but the IgM^+ memory B cells gradually disappeared (**Fig. 2M, 2N, 2O**), and IgG^+ spike-specific memory B cells then dominated by 6 months PSO (**Fig. 2O**). IgA^+

spike-specific memory B cells were detected as a small fraction of the total spike-specific memory B cells (~5%, **Fig. 2O**). IgG$^+$ spike-specific memory B cell frequency increased while IgA$^+$ was low and stable over the 8 month period (**Fig. 2I-2L**). Similar patterns of increasing IgG$^+$ memory, short-lived IgM$^+$ memory, and stable IgA$^+$ memory were observed for RBD- and nucleocapsid-specific memory B cells over the 8 month period (**Fig. 2O-2Q, Fig. S2E-S2H**).

There is limited knowledge of memory B cell kinetics following primary acute viral infection in humans. We are not aware of other cross-sectional or longitudinal analyses of antigen-specific memory B cells covering a 6+ month window after an acute infection by flow cytometry, except for four individuals with Ebola (*51*) and two individuals studied after yellow fever virus immunization (*52*), and also excepting influenza vaccines, for which people have repeated exposures and complex immune history. In the yellow fever study, short-lived IgM$^+$ memory and longer-lasting isotype-switched memory B cells were observed in the two individuals. Overall, based on the observations here, development of B cell memory to SARS-CoV-2 appeared to be robust and likely long-lasting.

SARS-CoV-2 memory CD8$^+$ T cells

SARS-CoV-2 memory CD8$^+$ T cells in 155 subjects were identified using a series of 23 peptide pools covering the entirety of the SARS-CoV-2 ORFeome (*2*, *5*). The most commonly recognized ORFs were spike (S), membrane (M), nucleocapsid (N), and ORF3a (CD69$^+$ CD137$^+$, **Fig. 3A** and Fig. S3A-B), consistent with our previous study (*2*). The percentage of subjects with detectable circulating SARS-CoV-2 memory CD8$^+$ T cells at 1 month PSO (d20-50) was 61% (30/49, **Fig. 3B**). The proportion of subjects positive for SARS-CoV-2 memory CD8$^+$ T cells at $\geq$ 6 months PSO was 50% (9/18). SARS-CoV-2 memory CD8$^+$ T cells declined with an apparent $t_{1/2}$ of 166d in the full cohort (**Fig. 3B**) and $t_{1/2}$ 139d among 24 paired samples (**Fig. 3C**). Spike-specific memory CD8$^+$ T cells exhibited similar kinetics to the overall SARS-CoV-2-specific memory CD8$^+$ T cells ($t_{1/2}$ 271d for the full cohort and 164d among paired samples, **Fig. 3D-E**, respectively). Phenotypic markers indicated that the majority of SARS-CoV-2-specific memory CD8$^+$ T cells were T_{EMRA} (*53*), with small populations of T_{CM} and T_{EM} (**Fig. 3F**). In the context of influenza, CD8$^+$ T_{EMRA} were associated with protection against severe disease in humans (*54*). The memory CD8$^+$ T cell half-lives observed herein were comparable to the 123d $t_{1/2}$ observed for memory CD8$^+$ T cells within 1-2 years after yellow fever immunization (*55*). Overall, the decay of circulating SARS-CoV-2-specific CD8$^+$ T cell is consistent with what has been reported for another acute virus.

SARS-CoV-2 memory CD4$^+$ T cells

SARS-CoV-2 memory CD4$^+$ T cells in 155 subjects were identified using the same series of 23 peptide pools covering the SARS-CoV-2 ORFeome (*2*, *5*). The most commonly recognized ORFs were spike, M, N, ORF3a, and nsp3 (CD137$^+$ OX40$^+$, **Fig. 4A** and Fig. S4A-B), consistent with our previous study (*2*). Circulating SARS-CoV-2 memory CD4$^+$ T cell responses were quite robust (**Fig. 4B**). Approximately one third (35%, 17/49) of COVID-19 cases at 1 month PSO had > 1.0% SARS-CoV-2-specific CD4$^+$ T cells. SARS-CoV-2 memory CD4$^+$ T cells declined over the 6 month time frame of this study with an apparent $t_{1/2}$ of 96d in the full cohort (**Fig. 4B**) and $t_{1/2}$ 64d among paired samples (**Fig. 4C**). The percentage of subjects with detectable circulating SARS-CoV-2 memory CD4$^+$ T cells at 1 month PSO (d20-50) was 94% (46/49, **Fig. 4B**). The proportion of subjects positive for SARS-CoV-2 memory CD4$^+$ T cells at $\geq$ 6 months PSO was 89% (16/18). Spike-specific and M-specific memory CD4$^+$ T cells exhibited similar kinetics to the overall SARS-CoV-2-specific memory CD4$^+$ T cells (whole cohort $t_{1/2}$ 150d and 174d, respectively. **Fig. 4D-E**, and Fig. S4D). A plurality of the SARS-CoV-2 memory CD4$^+$ T cells present at $\geq$ 6 months PSO were T_{CM} (**Fig. 4F**).

T follicular helpers (T_{FH}) are the specialized subset of CD4$^+$ T cells required for B cell help (*56*), and, therefore, critical for the generation of neutralizing antibodies and long-lived humoral immunity in

most contexts. Thus, we examined circulating T_{FH} (cT_{FH}) memory $CD4^+$ T cells, with particular interest in spike-specific memory cT_{FH} cells due to the importance of antibody responses against spike. Memory cT_{FH} cells specific for predicted epitopes across the remainder of the SARS-CoV-2 genome were also measured, using the MP_R megapool (*2*). Memory cT_{FH} cells specific for SARS-CoV-2 spike and MP_R were detected in the majority of COVID-19 cases at early time points (16/17 & 17/17. **Fig. 4G-H**, and Fig. S5A-C). cT_{FH} memory appeared to be stable, with 100% of subjects positive for spike cT_{FH} and 92% positive for MP_R cT_{FH} memory at 6 months PSO (**Fig. 4G-H**).

Recently activated cT_{FH} cells are PD-1^{hi} (*56*). Consistent with conversion to resting memory cT_{FH} cells, the percentage of PD-1^{hi} SARS-CoV-2-specific memory cT_{FH} dropped over time (**Fig. 4I**). $CCR6^+$ SARS-CoV-2-specific cT_{FH} cells have been associated with reduced COVID-19 disease severity (*5*) and have been reported to be a major fraction of spike-specific cT_{FH} cells (*5*, *57*). Here we confirmed that a significant fraction of both spike-specific and MP_R cT_{FH} were $CCR6^+$. We also observed significant increases in the fraction of $CCR6^+$ cT_{FH} memory over time ($P < 0.001$ and $P < 0.01$ compared to bulk cT_{FH} at $\geq$ 6 months PSO. **Fig. 4J**). Overall, substantial cT_{FH} memory was observed after SARS-CoV-2 infection, with durability $\geq$ 6 months PSO.

Immune memory relationships

Additional features of immune memory to SARS-CoV-2 were considered, including relationships between the compartments of immune memory. Immune memory was examined for associations between magnitude of memory and disease severity. Circulating antibody titers of severe COVID-19 cases trended higher, consistent with other studies (Fig. S6A). No distinction was observed in B and T cell memory between hospitalized and non-hospitalized COVID-19 cases (Fig. S6B-F), though interpretations are limited by the relatively low number of severe cases in this cohort. The influence of gender on immune memory was also assessed. Overall, males had higher spike IgG (ANCOVA p=0.00019, **Fig. 5A**) and nucleocapsid and RBD IgG (**Fig. S7A-D**). Higher spike IgG in males was also observed in another convalescent cohort (*48*). In contrast, no differences were observed in SARS-CoV-2 memory B cell frequencies or T cells between males and females (**Fig. S7E-I**). In sum, the heterogeneity in immune memory to SARS-CoV-2 was not primarily attributable to gender or COVID-19 disease severity.

Very few published data sets compare antigen-specific antibody, B cell, $CD8^+$ T cell, and $CD4^+$ T cell memory to an acute viral infection in the same individuals. To our knowledge, this is the largest study of its kind, for any acute infection. We examined relationships between immune memory compartments to gain insights into the interrelationships between immune memory types and better interpret the totality of immune memory to SARS-CoV-2. We focused on RBD IgG, RBD IgA, RBD memory B cells, total SARS-CoV-2-specific $CD8^+$ T cells, and total SARS-CoV-2-specific $CD4^+$ T cells, due to their putative potential roles in protective immunity. The majority (59%) of COVID-19 cases were positive for all five of these immune memory compartments at 1-2 months PSO (**Fig. 5B**), with the incomplete responses largely reflecting individuals with no detectable $CD8^+$ T cell memory and/or poor RBD IgA responses (**Fig. 5C**). By 5+ months after COVID-19, the proportion of individuals positive for all five of these immune memory compartments had dropped to 40%; nevertheless, 96% of individuals were still positive for at least three out of five SARS-CoV-2 immune memory responses (**Fig. 5B**). Immune memory at 5+ months PSO represented different contributions by immune memory compartments in different individuals (**Fig. 5C**), again demonstrating heterogeneity of immune memory, with increasing heterogeneity in the population over time.

Interrelationships between the components of memory were examined by assessing ratios over time. The ratio of SARS-CoV-2 $CD4^+$ and $CD8^+$ T cell memory was largely stable over time (**Fig. 5D**, Fig. S8A). Given that serological measurements are the simplest measurements of immune memory at a

population scale, we examined how well such measurements may serve as surrogate markers of other components of SARS-CoV-2 immune memory over time. The relationship between circulating RBD IgG and RBD-specific memory B cells changed ~20-fold over the time range studied (R=0.60, **Fig. 5D,** Fig. S8B). The changing relationship between circulating RBD IgA and RBD-specific memory B cells was even larger, with a 40-fold shift (R=0.62, **Fig. 5D,** Fig. S8C). The relationship between RBD IgG and SARS-CoV-2 $CD4^+$ T cell memory was relatively flat over the time range studied (**Fig. 5D**); however, variation spanned a ~1000-fold range and thus predictive power of circulating RBD IgG for assessing T cell memory was poor due to heterogeneity between individuals (R=0.02, Fig. S8D-E). In aggregate, while heterogeneity of immune responses is a defining feature of COVID-19, immune memory to SARS-CoV-2 develops in almost all subjects, with complex relationships between the individual immune memory compartments.

Conclusion

In this study, we aimed to fill a gap in our basic understanding of immune memory after COVID-19. This required simultaneous measurement of circulating antibodies, memory B cells, $CD8^+$ T cells, and $CD4^+$ T cells specific for SARS-CoV-2, in a group of subjects with a full range of disease and distributed from short time points PSO out to $\geq$ 8 months PSO. To our knowledge, this is the first study of its kind, incorporating antigen-specific antibody, memory B cell, $CD8^+$ T cell, and $CD4^+$ T cell measurements, out past 6 months post-infection. By studying these multiple compartments of adaptive immunity in an integrated manner, we observed that each component of SARS-CoV-2 immune memory exhibited distinct kinetics.

The spike IgG titers were durable, with modest declines in titers at 6 to 8 months PSO at the population level. RBD IgG and SARS-CoV-2 PSV neutralizing antibody titers were potentially similarly stable, consistent with the RBD domain of spike being the dominant neutralizing antibody target. However, due to the nature of only having data at two time points, the paired sample longitudinal data set could not distinguish between models of a continuous log-linear decay and a bi-phasic decay with a slower half-life later. It is well recognized that the magnitude of the antibody response against SARS-CoV-2 is highly heterogenous between individuals. We observed that heterogenous initial antibody responses did not collapse into a homogeneous circulating antibody memory. That heterogeneity is thus a central feature of immune memory to this virus. For antibodies, the responses spanned a ~200-fold range. Additionally, the heterogeneity showed that long-term longitudinal studies will be required to precisely define antibody kinetics to SARS-CoV-2. Nevertheless, at 5+ months PSO, almost all individuals were positive for SARS-CoV-2 spike and RBD IgG.

Notably, memory B cells specific for spike or RBD were detected in almost all COVID-19 cases, with no apparent half-life at 5+ months post-infection. B cell memory to some other infections has been observed to be long-lived, including 60+ years after smallpox vaccination (*58*), or 90+ years after infection with influenza (*59*), another respiratory virus like SARS-CoV-2. The memory T cell half-lives observed over 6+ months PSO in this cohort (~166-271d for $CD8^+$ and ~96-174d for $CD4^+$ T cells) were comparable to the 123d $t_{1/2}$ observed for memory $CD8^+$ T cells soon after yellow fever immunization (*55*). Notably, the durability of a fraction of the yellow fever virus-specific memory $CD8^+$ T cells possessed an estimated $t_{1/2}$ of 485d by deuterium labeling (*55*). Using different approaches, the long-term durability of memory $CD4^+$ T cells to smallpox, over a period of many years, was an estimated $t_{1/2}$ of ~10 years (*58*, *60*), which is also consistent with recent detection of SARS-CoV T cells 17 years after the initial infection (*61*). These data suggest that T cell memory might reach a more stable plateau, or slower decay phase, later than the first 6 months post-infection.

While immune memory is the source of long-term protective immunity, direct conclusions about protective immunity cannot be made on the basis of quantifying SARS-CoV-2 circulating antibodies,

memory B cells, $CD8^+$ T cells, and $CD4^+$ T cells, because mechanisms of protective immunity against SARS-CoV-2 or COVID-19 are not defined in humans. Nevertheless, some reasonable interpretations can be made. Antibodies are the only component of immune memory that can provide truly sterilizing immunity. Immunization studies in non-human primates have indicated that circulating neutralization titers of ~200 may provide sterilizing immunity against a relatively high dose URT challenge (*62*), and neutralizing titers of ~3,400 may provide sterilizing immunity against a very high dose URT challenge (*63*), although direct comparisons are not possible because the neutralizing antibody assays have not been standardized (*3*). Conclusions are also constrained by the limited overall amount of data on the topic of protective immunity to SARS-CoV-2, though progress in this field has been exceptionally rapid by any standard.

Beyond sterilizing immunity, confining SARS-CoV-2 to the URT and oral cavity would minimize COVID-19 disease severity to 'common cold' or asymptomatic disease. This outcome is the primary goal of current COVID-19 vaccine clinical trials (*3*, *64*). Such an outcome could potentially be mediated by a mixture of memory $CD4^+$ T cells, memory $CD8^+$ T cells, and memory B cells specific for RBD producing anamnestic neutralizing antibodies, based on mechanisms of action demonstrated in mouse models of other viral infections (*65–67*). In human COVID-19 infections, SARS-CoV-2-specific $CD4^+$ T cells and $CD8^+$ T cells are associated with lessened COVID-19 disease severity of an ongoing SARS-CoV-2 infection (*5*), and rapid seroconversion was associated with significantly reduced viral loads in acute disease over 14 days (*30*). Both of those associations are consistent with the hypothesis that SARS-CoV-2 memory T cells and B cells would be capable of substantially limiting SARS-CoV-2 dissemination and/or cumulative viral load, resulting in substantially reduced COVID-19 disease severity. The likelihood of such outcomes is also closely tied to the kinetics of the infection, as memory B and T cell responses can take 3-5 days to successfully respond to an infection. As noted above, given the relatively slow course of severe COVID-19 in humans, a large window of time is available for resting immune memory compartments to potentially contribute in meaningful ways to protective immunity against pneumonia or severe or fatal 2° COVID-19. The presence of sub-sterilizing neutralizing antibody titers at the time of SARS-CoV-2 exposure would blunt the size of the initial infection, and may provide an added contribution to limiting COVID-19 severity, based on observations of protective immunity for other human respiratory viral infections (*38*, *68–70*) and observations of SARS-CoV-2 vaccines in non-human primates (*49*, *63*, *71*).

This study has limitations. Longitudinal data for each subject, with at least 3 time points per subject, would be required to distinguish between linear, one-phase with plateau, and two-phase decay best fit models for more precise understanding of long-term kinetics of SARS-CoV-2 antibodies. Nevertheless, the current cross-sectional data describe well the dynamics of SARS-CoV-2 memory B cells, $CD8^+$ T cell, and $CD4^+$ T cell over 6 months PSO. Additionally, circulating memory was assessed here; it is possible that local URT immune memory is a minimal, moderate, or large component of immune memory after a primary infection with SARS-CoV-2. This remains to be determined.

When considering potential connections between immune memory and protective immunity, it is key to consider the available epidemiological data. Individual case reports demonstrate that reinfections with SARS-CoV-2 are occurring (*72*, *73*). What is currently lacking is an epidemiological framework for quantifying how rare or common such reinfection events are. Thus, interpretations of current events are very constrained. There is a high degree of heterogeneity in the magnitude of adaptive immune responses to this novel coronavirus. That heterogeneity was observed in this study to be carried on into the immune memory phase to SARS-CoV-2. As a result of the immune response heterogeneity, as observed in the cohort here, it may be expected that at least a fraction of the SARS-CoV-2-infected population with particularly low immune memory would be susceptible to re-infection relatively quickly. The source of heterogeneity in immune memory to SARS-CoV-2 is unknown and worth further examination. It is possible that some of that heterogeneity is a result of low cumulative viral load

or initial inoculum, essentially resulting in a very minor or transient infection that barely triggered an adaptive immune response in some individuals. Nevertheless, immune memory consisting of at least three immunological compartments was measurable in ~90% of subjects $\geq$ 5 months PSO, indicating that durable immunity against 2° COVID-19 disease is a possibility in most individuals.

METHODS

Human Subjects

The Institutional Review Boards of the University of California, San Diego (UCSD; 200236X) and the La Jolla Institute for Immunology (LJI; VD-214) approved the protocols used for blood collection for subjects with COVID-19 who donated at all sites other than Mt. Sinai. The Icahn School of Medicine at Mt. Sinai IRB approved the samples collected at this institution in New York City (IRB-16-00791). All human subjects were assessed for medical decision-making capacity using a standardized, approved assessment, and voluntarily gave informed consent prior to being enrolled in the study. Study inclusion criteria included a diagnosis of COVID-19 or suspected COVID-19, age of 18 years or greater, willingness and ability to provide informed consent. Although not a strict inclusion criterion, evidence of positive PCR-based testing for SARS-CoV-2 was requested from subjects prior to participation. 143 cases were confirmed SARS-CoV-2 positive by PCR-based testing (Table S1). Two subjects tested negative by SARS-CoV-2 PCR (Table S1). The remainder were not tested or did not have test results available for review (Table S1). Subjects who had a medical history and/or symptoms consistent with COVID-19, but lacked positive PCR-based testing for SARS-CoV-2 and subsequently had negative laboratory-based serologic testing for SARS-CoV-2 were then excluded; i.e., all COVID-19 cases in this study were confirmed cases by SARS-CoV-2 PCR or SARS-CoV-2 serodiagnostics, or both. Adults of all races, ethnicities, ages, and genders were eligible to participate. Study exclusion criteria included lack of willingness to participate, lack of ability to provide informed consent, or a medical contraindication to blood donation (e.g. severe anemia). Subject samples at LJI were obtained from individuals in California and at least seven other states.

Blood collection and processing methods at LJI were performed as previously described (*5*). Briefly, whole blood was collected via phlebotomy in acid citrate dextrose (ACD) serum separator tubes (SST), or ethylenediaminetetraacetic acid (EDTA) tubes and processed for peripheral blood mononuclear cells (PBMC), serum, and plasma isolation. Most donors were screened for symptoms prior to scheduling blood draws, and had to be symptom-free and approximately 3-4 weeks out from symptom onset at the time of the initial blood draw at UCSD or LJI, respectively. Samples were coded, and then de-identified prior to analysis. Other efforts to maintain the confidentiality of participants included the labeling samples with coded identification numbers. An overview of the characteristics of subjects with COVID-19 is provided in Table S1.

COVID-19 disease severity was scored from 0 to 10 using a numerical scoring system based on the NIH ordinal scale (*5*, *74*). A categorical descriptor was applied based on this scoring system: "asymptomatic" for a score of 1, "mild" for a score of 2-3, "moderate" for a score of 4-5, and "severe" for a score of 6 or more. Subjects with a numerical score of 4 or higher required hospitalization (including admission for observation) for management of COVID-19. The days PSO was determined based on the difference between the date of the blood collection and the date of first reported symptoms consistent with COVID-19. For asymptomatic subjects, the day from first positive SARS-CoV-2 PCR-based testing was used in place of the date of first reported COVID-19 symptoms.

SARS-CoV-2 ELISAs

SARS-CoV-2 ELISAs were performed as previously described (*2*, *5*, *75*). Briefly, Corning 96-well half area plates (ThermoFisher 3690) were coated with 1μg/mL of antigen overnight at 4°C. Antigens included recombinant SARS-CoV-2 RBD protein, recombinant spike protein (*5*), and recombinant nucleocapsid protein (GenScript Z03488). The following day, plates were blocked with 3% milk in phosphate buffered saline (PBS) containing 0.05% Tween-20 for 1.5 hours at room temperature. Plasma was heat inactivated at 56°C for 30-60 minutes. Plasma was diluted in 1% milk containing 0.05% Tween-20 in PBS starting at

a 1:3 dilution followed by serial dilutions by 3 and incubated for 1.5 hours at room temperature. Plates were washed 5 times with 0.05% PBS-Tween-20. Secondary antibodies were diluted in 1% milk containing 0.05% Tween-20 in PBS. For IgG, anti-human IgG peroxidase antibody produced in goat (Sigma A6029) was used at a 1:5,000 dilution. For IgA, anti-human IgA horseradish peroxidase antibody (Hybridoma Reagent Laboratory HP6123-HRP) was used at a 1:1,000 dilution. The HP6123 monoclonal anti-IgA was used because of its CDC and WHO validated specificity for human IgA1 and IgA2 and lack of crossreactivity with non-IgA isotypes (*76*).

Endpoint titers were plotted for each sample, using background subtracted data. A positive control standard was created by pooling plasma from 6 convalescent COVID-19 donors to normalize between experiments. The limit of detection (LOD) was defined as 1:3 for IgG, 1:10 for IgA. Limit of sensitivity (LOS) for SARS-CoV-2 infected individuals was established based on uninfected subjects, using plasma from normal healthy donors never exposed to SARS-CoV-2. For cross-sectional analyses, modeling for the best fit curve (e.g., one phase decay versus simple linear regression) was performed using GraphPad Prism 8.0. Best curve fit was defined by an extra sum-of-squares F Test, selecting the simpler model unless $P < 0.05$ (*77*). To calculate the $t_{1/2}$, $\log_2$ transformed data was utilized. Using the best fit curve, either a one phase decay non-linear fit or a simple linear regression (-1/slope) was utilized. Pearson R was calculated for correlation. For longitudinal samples, a simple linear regression was performed, with $t_{1/2}$ calculated from $\log_2$ transformed data for each pair. For gender analyses, modeling and $t_{1/2}$ was performed similar to cross-sectional analyses; ANCOVA (VassarStats or GraphPad Prism 8.4) was then performed between male and female data sets.

Neutralizing antibody assays

The pseudovirus neutralizing antibody assay was performed as previously described (*5*). Briefly, Vero cells were seeded in 96 well plates to produce a monolayer at the time of infection. Pre-titrated amounts of rVSV-SARS-Cov-2 (phCMV3-SARS-CoV-2 spike SARS-CoV-2-pseduotyped VSV-ΔG-GFP were generated by transfecting 293T cells) were incubated with serially diluted human plasma at 37°C for 1 hour before addition to confluent Vero monolayers in 96-well plates. Cells were incubated for 12-16 hours at 37°C in 5% CO_2. Cells were then fixed in 4% paraformaldehyde, stained with 1ug/mL Hoechst, and imaged using a CellInsight CX5 imager to quantify total number of cells expressing GFP. Infection was normalized to the average number of cells infected with rVSV-SARS-CoV-2 incubated with normal human plasma. The limit of detection (LOD) was established as < 1:20 based on plasma samples from a series of unexposed control subjects. Data are presented as the relative infection for each concentration of sera. Neutralization IC50 titers were calculated using One-Site Fit LogIC50 regression in GraphPad Prism 8.0.

Detection of antigen-specific memory B cells

To detect SARS-CoV-2 specific B cells, biotinylated protein antigens were individually multimerized with fluorescently labeled streptavidin at 4°C for one hour. Full-length SARS-CoV-2 spike (2P-stabilized, double Strep-tagged) and RBD were generated in-house. Biotinylation was performed using biotin-protein ligase standard reaction kit (Avidity, Cat# Bir500A) following the manufacturers standard protocol and dialyzed over-night against PBS. Biotinylated spike was mixed with streptavidin BV421 (BioLegend, Cat# 405225) and streptavidin Alexa Fluor 647 (Thermo Fisher Scientific, Cat# S21374) at 20:1 ratio (~6:1 molar ratio). Biotinylated RBD was mixed with streptavidin PECy7 (BioLegend, Cat# 405206) at 2.2:1 ratio (~4:1 molar ratio). Biotinylated SARS-CoV-2 full length nucleocapsid (Avi- and His-tagged; Sino Biological, Cat# 40588-V27B-B) was multimerized using streptavidin PE (BioLegend, Cat# 405204) and streptavidin BV711 (BioLegend, Cat# 405241) at 5.5:1 ratio (~6:1 molar ratio). Streptavidin PECy5.5 (Thermo Fisher Scientific, Cat# SA1018) was used as a decoy probe to gate out SARS-CoV-2

non-specific streptavidin-binding B cells. The antigen probes prepared individually as above were then mixed in Brilliant Buffer (BD Bioscience, Cat# 566349) containing 5μM free d-biotin (Avidity, Cat# Bir500A). Free d-biotin ensured minimal cross-reactivity of antigen probes. ~10^7 previously frozen PBMC samples were prepared in U-bottom 96-well plates and stained with 50μL antigen probe cocktail containing 100ng spike per probe (total 200ng), 27.5ng RBD, 40ng nucleocapsid per probe (total 80ng) and 20ng streptavidin PECy5.5 at 4°C for one hour to ensure maximal staining quality before surface staining with antibodies as listed in Table S2 was performed in Brilliant Buffer at 4°C for 30min. Dead cells were stained using LIVE/DEAD Fixable Blue Stain Kit (Thermo Fisher Scientific, Cat# L34962) in DPBS at 4°C for 30min. ~80% of antigen-specific memory (IgD^- and/or $CD27^+$) B cells detected using this method were IgM^+, IgG^+, or IgM^- IgG^- IgA^+, which were comparable to non-specific memory B cells. Based on these observations, we concluded that the antigen probes did not significantly impact the quality of surface immunoglobulin staining. Stained PBMC samples were acquired on Cytek Aurora and analyzed using FlowJo10.7.1 (BD Bioscience). Frequency of antigen-specific memory B cells were expressed as a percentage of total B cells ($CD19^+$ $CD20^+$ $CD38^{int/-}$, $CD3^-$, $CD14^-$, $CD16^-$, $CD56^-$, $LIVE/DEAD^-$, lymphocytes), or as numbers per 10^6 PBMC ($LIVE/DEAD^-$ cells). LOD was set based on median + 2×SD of [1 / (number of total B cells recorded)] or median + 2×SD of [10^6 / (number of PBMC recorded)]. LOS was set as the median + 2×SD of the results in unexposed donors. Phenotype analysis of antigen-specific B cells was performed only in subjects with at least 10 cells detected in the respective antigen-specific memory B cell gate. In each experiment, PBMC from a known positive control (COVID-19 convalescent subject) and unexposed subjects were included to ensure consistent sensitivity and specificity of the assay. For each data set, second order polynomial, simple linear regression, and pseudo-first order kinetic models were considered. The model with a lower Akaike's Information Criterion value was determined to be better-fit and visualized.

Activation induced markers (AIM) T cell assay

Antigen-specific $CD4^+$ T cells were measured as a percentage of AIM^+ ($OX40^+CD137^+$) $CD4^+$ T and ($CD69^+CD137^+$) $CD8^+$ T cells after stimulation of PBMCs with overlapping peptide pools spanning the entire ORFeome, as previously described (*2*). Cells were cultured for 24 hours in the presence of SARS-CoV-2 specific MPs [1 μg/mL] or 5 μg/mL phytohemagglutinin (PHA, Roche) in 96-wells U-bottom plates at $1x10^6$ PBMCs per well. A stimulation with an equimolar amount of DMSO was performed as negative control, PHA, and stimulation with a combined CD4 and CD8 cytomegalovirus MP (CMV, 1 μg/mL) were included as positive controls. Any sample with low PHA signal was excluded as a quality control. Antigen-specific $CD4^+$ and $CD8^+$ T cells were measured as background (DMSO) subtracted data, with a minimal DMSO level set to 0.005%. All positive ORFs (> 0.02% for CD4s, > 0.05% for CD8s) were then aggregated into a combined sum of SARS-CoV-2-specific $CD4^+$ or $CD8^+$ T cells. The threshold for positivity for antigen-specific $CD4^+$ T cell responses (0.03%) and antigen-specific $CD8^+$ T cell responses (0.12%) has been calculated using the median two-fold standard deviation of all negative controls measured (>150). The antibody panel utilized in the ($OX40^+CD137^+$) $CD4^+$ T and ($CD69^+CD137^+$) $CD8^+$ T cells AIM staining is shown in Table S2.

For surface $CD40L^+$ $OX40^+$ $CD4^+$ T cell AIM assays, experiments were performed as previously described (*5*), with the following modifications. Cells were cultured in complete RPMI containing 5% Human AB Serum (Gemini Bioproducts), 2Me, PenStrep, NaPy, and NE-AA. Prior to addition of peptide MPs, cells were blocked at 37C for 15 minutes with 0.5ug/mL anti-CD40 mAb (Miltenyi Biotec).

ACKNOWLEDGEMENTS

We would like to thank the LJI Clinical Core, specifically Gina Levi, RN and Brittany Schwan for healthy donor enrollment and blood sample procurement. We are also grateful to the Mt. Sinai Personalized

Virology Initiative for sharing banked samples from study participants with COVID-19. We are grateful to Dr. A. Wajnberg for study participant referrals and to the Personalized Virology Initiative (Dr. G. Kleiner, Dr. LCF Mulder, Dr. M. Saksena, K. Srivastava, C. Gleason, C. M. Bermúdez-González, K. Beach, K. Russo, L. Sominsky, E. Ferreri, R. Chernet, L. Eaker, A. Salimbangon, D. Jurczyszak, H. Alshammary, W. Mendez, A. Amoako, S. Fabre, S. Suthakaran, M. Awawda, E. Hirsch, A. Shin) for sharing banked samples from study participants with COVID-19. This work was funded by the NIH NIAID under awards AI142742 (Cooperative Centers for Human Immunology) (A.S., S.C.), NIH contract Nr. 75N9301900065 (D.W., A.S.), U01 AI141995-03 (A.S., P.B.), and U01 CA260541-01 (D.W). This work was additionally supported in part by the John and Mary Tu Foundation (D.S.), the NIAID under K08 award AI135078 (J.D.), UCSD T32s AI007036 and AI007384 Infectious Diseases Division (S.Ram., S.Raw.), and the Bill and Melinda Gates Foundation INV-006133 from the Therapeutics Accelerator, Mastercard, Wellcome, private philanthropic contributions (K.H., E.O.S., S.C.), and a FastGrant from Emergent Ventures in aid of COVID-19 research. This work was partially supported by the NIAID Centers of Excellence for Influenza Research and Surveillance (CEIRS) contract HHSN272201400008C (F.K., for reagent generation), the Collaborative Influenza Vaccine Innovation Centers (CIVIC) contract 75N93019C00051 and the generous support of the JPB foundation (F.K., V.S.), the Cohen Foundation (VS, FK), the Open Philanthropy Project (#2020-215611; F.K., V.S.), as well as other philanthropic donations. We would also like to thank all of the COVID-19 and healthy human subjects who made this research possible through their generous blood donations.

COMPETING INTERESTS

A.S. is a consultant for Gritstone, Flow Pharma, Merck, Epitogenesis, Gilead and Avalia. S.C. is a consultant for Avalia. LJI has filed for patent protection for various aspects of T cell epitope and vaccine design work. Mount Sinai has licensed serological assays to commercial entities and has filed for patent protection for serological assays. D.S., F.A., V.S. and F.K. are listed as inventors on the pending patent application (F.K., V.S.), and Newcastle disease virus (NDV)-based SARS-CoV-2 vaccines that name F.K. as inventor. All other authors declare no conflict of interest.

FIGURE LEGENDS

Figure 1. SARS-CoV-2 circulating antibodies over time. (A) Cross-sectional spike IgG from COVID-19 subject plasma samples (n=228). Linear decay preferred model for best fit curve, $t_{1/2}$ = 140d, 95% CI: 89-329 days. R = -0.20, p=0.003. **(B)** Longitudinal spike IgG (n=50), average $t_{1/2}$ 100d, 95% CI: 64-220d **(C)** Cross-sectional RBD IgG. Linear decay preferred model for best fit curve, $t_{1/2}$ = 83d, 95% CI: 62 to 127d. R = -0.34, p<0.0001. **(D)** Longitudinal RBD IgG, average $t_{1/2}$ of 68d, 95% CI: 57-86d **(E)** Cross-sectional PSV neutralizing titers. One-phase decay (blue line) preferred model for best fit curve, $t_{1/2}$ = 27d, 95%: CI: 11 to 153d. R = -0.27, p <0.0001. Linear fit shown as black line. **(F)** Longitudinal PSV neutralizing titers of SARS-CoV-2 infected subjects, average $t_{1/2}$ 87d, 95% CI: 68-123d **(G)** Cross-sectional nucleocapsid IgG. Linear decay preferred model for best fit curve, $t_{1/2}$ = 67d, 95% CI: 49-105d. R = -0.32, p<0.0001. **(H)** Longitudinal nucleocapsid IgG, average $t_{1/2}$ was 67d, 95% CI: 54-88d. **(I)** Cross-sectional Spike IgA titers. One-phase decay (blue line) preferred model for best fit curve, $t_{1/2}$ = 11d, 95%: CI: 5 to 25d. R = -0.14, p=0.04. Linear fit shown as black line. **(J)** Longitudinal Spike IgA, $t_{1/2}$ = 214d, 95% CI 126-703d. **(K)** Cross-sectional RBD IgA. One phase decay (blue line) preferred model for best fit curve, $t_{1/2}$ = 27d, 95% CI: 15 to 58d. R = -0.40, p<0.0001. Linear fit shown in black. **(L)** Longitudinal RBD IgA, average $t_{1/2}$ was 72d, 95% CI: 55-104d. For cross-sectional analyses, SARS-CoV-2 infected subjects (white circles, n=238) and unexposed subjects (gray circles, n=51). For longitudinal samples, SARS-CoV-2 subjects (n=50). The dotted black line indicates limit of detection (LOD). The dotted green line indicates limit of sensitivity (LOS) above uninfected controls. Unexposed = gray, COVID subjects = white. Thick blue line represents best fit curve. When two fit curves are shown, the thin black line represents the alternative fit curve.

Figure 2. Kinetics of SARS-CoV-2 memory B cell responses. (**A**) Example plots showing staining patterns of SARS-CoV-2 antigen probes on memory B cells (See Fig S1 for gating). One unexposed donor and three convalescent COVID-19 subjects are shown. Numbers indicate percentages. (**B**) Gating strategies to define IgM^+, IgG^+, or IgA^+ SARS-CoV-2 spike-specific memory B cells. The same gating strategies were used for RBD- or nucleocapsid-specific B cells. (**C**) Cross-sectional analysis of frequency (% of $CD19^+$ $CD20^+$ B cells) of SARS-CoV-2 S-specific total (IgG^+, IgM^+, or IgA^+) memory B cells. Pseudo-first order kinetic model for best fit curve (R^2 = 0.14). (**D**) Longitudinal analysis of SARS-CoV-2 spike-specific memory B cells. (**E**) Cross-sectional analysis of SARS-CoV-2 RBD-specific total (IgG^+, IgM^+, or IgA^+) memory B cells. Second order polynomial model for best fit curve (R^2 = 0.21). (**F**) Longitudinal analysis of SARS-CoV-2 RBD-specific memory B cells. (**G**) Cross-sectional analysis of SARS-CoV-2 nucleocapsid-specific total (IgG^+, IgM^+, or IgA^+) memory B cells. Pseudo-first order kinetic model for best fit curve (R^2 = 0.19). (**H**) Longitudinal analysis of IgG^+ SARS-CoV-2 spike-specific memory B cells. (**I**) Cross-sectional analysis of SARS-CoV-2 spike-specific IgG^+ memory B cells. Pseudo-first order kinetic model for best fit curve (R^2 = 0.24). (**J**) Longitudinal analysis of SARS-CoV-2 spike-specific IgG^+ memory B cells. (**K**) Cross-sectional analysis of SARS-CoV-2 spike-specific IgA^+ memory B cells. Second order polynomial model for best fit curve (R^2 = 0.10). (**L**) Longitudinal analysis of SARS-CoV-2 spike-specific IgA^+ memory B cells. (**M**) Cross-sectional analysis of SARS-CoV-2 spike-specific IgM^+ memory B cells. Second order polynomial model for best fit curve (R^2 = 0.17). (**N**) Longitudinal analysis of SARS-CoV-2 spike-specific IgM^+ memory B cells. (**O**) Fraction of SARS-CoV-2 antigen-specific memory B cells that belong to indicated Ig isotypes at 1-8 months PSO. (**P**) Cross-sectional analysis of SARS-CoV-2 RBD-specific IgG^+ memory B cells. Second order polynomial model for best fit curve (R^2 = 0.27). (**Q**) Cross-sectional analysis of SARS-CoV-2 nucleocapsid-specific IgG^+ memory B cells. Second order polynomial model for best fit curve (R^2 = 0.26). n = 20 unexposed subjects (gray circles) and n = 180 COVID-19 subjects (n = 217 data points, white circles) for cross-sectional analysis. n = 36 COVID-19 subjects (n =

73 data points, white circles) for longitudinal analysis. The dotted black line indicates limit of detection (LOD). The dotted green line indicates limit of sensitivity (LOS).

Figure 3. SARS-CoV-2 memory CD8$^+$ T cells. (A) Representative flow cytometry plots of SARS-CoV-2-specific CD8$^+$ T cells (CD69$^+$ CD137$^+$, See Fig S3 for gating) after overnight stimulation with S, N, M, ORF3a, or nsp3 peptide pools, compared to negative control (DMSO). **(B)** Cross-sectional analysis of frequency (% of CD8$^+$ T cells) of total SARS-CoV-2-specific CD8$^+$ T cells. **(C)** Longitudinal analysis of total SARS-CoV-2-specific CD8$^+$ T cells in paired samples from the same subjects. **(D)** Cross-sectional analysis of spike-specific CD8$^+$ T cells. **(E)** Longitudinal analysis of spike-specific CD8$^+$ T cells in paired samples from the same subjects. **(F)** Distribution of T_{CM}, T_{EM}, and T_{EMRA} among total SARS-CoV-2-specific CD8$^+$ T cells. n = 155 COVID-19 subject samples (white circles) for cross-sectional analysis. n = 30 COVID-19 subjects (white circles) for longitudinal analysis. The dotted black line indicates limit of detection (LOD).

Figure 4. SARS-CoV-2 memory CD4$^+$ T cells. (A) Representative flow cytometry plots of SARS-CoV-2-specific CD4$^+$ T cells (CD137$^+$ OX40$^+$, See Fig S4 for gating) after overnight stimulation with S, N, M, ORF3a, or nsp3 peptide pools, compared to negative control (DMSO). **(B)** Cross-sectional analysis of frequency (% of CD4$^+$ T cells) of total SARS-CoV-2-specific CD4$^+$ T cells. **(C)** Longitudinal analysis of total SARS-CoV-2-specific CD4$^+$ T cells in paired samples from the same subjects. **(D)** Cross-sectional analysis of spike-specific CD4$^+$ T cells. **(E)** Longitudinal analysis of spike-specific CD4$^+$ T cells in paired samples from the same subjects. **(F)** Distribution of T_{CM}, T_{EM}, and T_{EMRA} among total SARS-CoV-2-specific CD4$^+$ T cells. (**G**, **H**) Quantitation of SARS-CoV-2-specific T_{FH} cells (surface CD40L$^+$ OX40$^+$, as % of CD4$^+$ T cells. See Fig S5 for gating) after overnight stimulation with **(G)** spike (S) or **(H)** MP_R peptide pools. (**I**) PD-1^{hi} SARS-CoV-2-specific T_{FH} at 1-2 months (mo) and 6 mo PSO. (**J**) CCR6$^+$ SARS-CoV-2-specific T_{FH} in comparison to bulk cT_{FH} cells in blood.
For A-F, n = 155 COVID-19 subject samples (white circles) for cross-sectional analysis. n = 30 COVID-19 subjects (white circles) for longitudinal analysis. The dotted black line indicates limit of detection (LOD). For G-J, n = 34 COVID-19 subject samples (white circles), n = 21 COVID-19 subjects at 1-2 mo, n = 13 COVID-19 subjects at 6 mo. The dotted black line indicates limit of detection (LOD).* $p<0.05$, **$p<0.01$, *** $p<0.001$, **** $p<0.0001$.

Figure 5. Immune memory relationships. (A) Relationship between gender and spike IgG titers over time. Males: One phase decay preferred model, $t_{1/2}$ = 23d, 95% CI: 7-224d, R = -0.26, p=0.0057. Females: linear decay preferred model, $t_{1/2}$ = 159d, 95% CI 88-847d, R = -0.18, p=0.05. **(B)** Immune memory to SARS-CoV-2 during the early phase (1-2 mo, black line), medium phase (3-4 mo, red line), or late phase (5+ mo, blue line). For each individual, a score of 1 was assigned for each response above LOS in terms of RBD-specific IgG, RBD-specific IgA, RBD-specific memory B cells, SARS-CoV-2 specific CD4$^+$ T cells, and SARS-CoV-2-specific CD8$^+$ T cells, giving a maximum total of 5 components of SARS-CoV-2 immune memory. Only COVID-19 convalescent subjects with all five immunological parameters tested were included in the analysis. n = 83 (1-2 mo), n = 53 (3-4 mo), n = 28 (5+ mo). **(C)** Percentage dot plots showing frequencies (normalized to 100%) of subjects with indicated immune memory components as described in (B) during the early (1-2 mo) or late (5+ mo) phase. "G", RBD-specific IgG. "B", RBD-specific memory B cells. "4", SARS-CoV-2 specific CD4$^+$ T cells. "8", SARS-CoV-2 specific CD8$^+$ T cells. "A", RBD-specific IgA. **(D)** Relationships between immune memory compartments in COVID-19 subjects over time, as ratios (full curves and data shown in Fig. S8). AU = arbitrary units, scaled from Fig. S8. "B:IgA", RBD-specific memory B cell ratio to RBD IgA antibodies. "B:IgG", RBD-specific memory B cell ratio to RBD IgG antibodies. "B:CD4", RBD-specific memory B cell ratio to SARS-CoV-2-specific CD4$^+$

T cells. "CD4:CD8", SARS-CoV-2-specific $CD4^+$ T cells ratio to SARS-CoV-2-specific $CD8^+$ T cells. "CD4:IgG", SARS-CoV-2-specific $CD4^+$ T cells ratio to RBD IgG antibodies.

SUPPLEMENTARY MATERIALS

Table S1. Participant characteristics

	COVID-19 (n = 185)
Age (years)	19-81 [Median = 40, IQR = 19.5]
Gender	
Male (%)	43% (79/185)
Female (%)	57% (106/185)
Race	
African American or Black (%)	3% (5/185)
Alaskan Native or American Indian (%)	1% (1/185)
Asian (%)	8% (14/185)
Native Hawaiian or Pacific Islander (%)	0% (0/185)
Multiracial (%)	1% (2/185)
Other (%)	1% (1/185)
Unknown (%)	10% (19/185)
White (%)	77% (143/185)
Ethnicity	
Hispanic or Latino (%)	15% (27/185)
Non-Hispanic (%)	80% (148/185)
Unknown (%)	5% (10/185)
Hospitalization status	
Never hospitalized (%)	92% (171/185)
Hospitalized (%)	7% (13/185)
Unknown if hospitalized (%)	1% (1/185)
Sample Collection Dates	March-October 2020
SARS-CoV-2 PCR Positivity	
Positive	77% (143/185)
Negative	1% (2/185)
Not performed	20% (37/185)
Unknown	2% (3/185)
Peak Disease Severity	
Asymptomatic (score 1)	2% (4/185)
Mild (non-hospitalized. Score 2-3)	90% (167/185)
Moderate (hospitalized. Score 4-5)	3% (6/185)
Severe (hospitalized. Score 6+)	4% (7/185)
Unknown	1% (1/185)
Days Post Symptom Onset at Collection; n = 233	6-240 (Median 90.5, IQR 99)
Blood Collection Frequency	
Multiple Time Point Donors (2-4 times)	21% (38/185)
Single Time Point Donors	79% (147/185)

Table S2. Memory B cell flow cytometry panel.

Reagents	SOURCE	IDENTIFIER
Mouse anti-human CD62L BV615 (clone SK11)	BD Bioscience	Cat# 565219
Mouse anti-human CD19 BUV563 (clone SJ25C1)	BD Bioscience	Cat# 612916
Mouse anti-human FCRL5 (CD307e) BUV615 (clone 509F6)	BD Bioscience	Cat# 751131
Mouse anti-human CD95 BUV737 (clone DX2)	BD Bioscience	Cat# 612790
Mouse anti-human CCR6 BUV805 (clone 11A9)	BD Biosicnece	Cat# 749361
Mouse anti-human CD138 BV480 (clone MI15)	BD Bioscience	Cat# 566140
Mouse anti-human IgD BV510 (clone IA6-2)	BioLegend	Cat# 348220
Mouse anti-human IgM BV570 (clone MHM-88)	BioLegend	Cat# 314517
Mouse anti-human CD24 BV605 (clone ML5)	BioLegend	Cat# 311124
Mouse anti-human CD20 BV650 (clone 2H7)	BioLegend	Cat# 302336
Rat anti-human CXCR5 BV750 (clone RF8B2)	BD Bioscience	Cat# 747111
Mouse anti-human CD71 BV786 (clone M-A712)	BD Bioscience	Cat# 563768
Mouse anti-human CD27 BB515 (clone M-T271)	BD Bioscience	Cat# 564642
Mouse anti-human IgA Vio Bright FITC (clone IS11-8E10)	Miltenyi Biotec	Cat# 130-113-480
Mouse anti-human CD3 PerCP (clone SK7)	BioLegend	Cat# 344814
Mouse anti-human CD14 PerCP (clone 63D3)	BioLegend	Cat# 367152
Mouse anti-human CD16 PerCP (clone 3G8)	BioLegend	Cat# 302030
Mouse anti-human CD56 PerCP (clone HCD56)	BioLegend	Cat# 318342
Rat anti-human IgG PerCP/Cyanine5.5 (clone M1310G05)	BioLegend	Cat# 410710
Mouse anti-human CD85j PE/Dazzle 594	BioLegend	Cat# 333716
Mouse anti-human CD11c PE/Cyanine5 (clone 3.9)	BioLegend	Cat# 301610
Mouse anti-human CD21 Alexa Fluor 700 (clone Bu32)	BioLegend	Cat# 354918

Table S3. Antibodies utilized in the CD8$^+$ and CD4$^+$ T cell activation induced markers (AIM) assays

Membrane Antibody	Fluorochrome	Clone/vendor/catalog	Dilution
CD45RA	BV421	HI100/BioLegend/304130	1:50
CD14	BUV563	M5E2/BD/741360	1:100
CD19	BUV805	HIB19/BD/742007	1:100
Live/Dead	ef506/Aqua	Thermo Fisher/65-0866-18	1:200
CD8	BV650	RPA-T8/BioLegend/301042	1:50
CD4	BV605	RPA-T4/BD/562658	1:25
CCR7	FITC	G043H7/BioLegend/353216	1:50
CD69	PE	FN50/BD/555531	1:10
OX40	PE-Cy7	Ber-ACT35/BioLegend/350012	1:50
CD137	APC	4B4-1/BioLegend/309810	1:25
CD3	AF700	UCHT1/Thermo Fisher/56-0038-42	1:25

SUPPLEMENTARY FIGURE LEGENDS

Figure S1. SARS-CoV-2 memory B cells. (**A**) Gating strategies to define spike-, RBD-, or nucleocapsid-specific memory B cells.

Figure S2. Kinetics of memory B cell responses. (**A**) Cross-sectional analysis showing SARS-CoV-2 Spike-specific memory B cell numbers per 10^6 PBMC. Second order polynomial model for best fit curve (R^2 = 0.14). **(B)** Percentage of Spike-specific B cells that are specific to RBD. Simple linear regression (R^2 = 0.024) (**C**) Cross-sectional analysis showing SARS-CoV-2 RBD-specific memory B cell numbers per 10^6 PBMC. Second order polynomial model for best fit curve (R^2 = 0.15). (**D**) Cross-sectional analysis showing SARS-CoV-2 nucleocapsid-specific memory B cell numbers per 10^6 PBMC. Second order polynomial model for best fit curve (R^2 = 0.14). (**E**) Cross-sectional analysis of frequency (% of $CD19^+$ $CD20^+$ B cells) of SARS-CoV-2 RBD-specific IgA^+ memory B cells. Second order polynomial model for best fit curve (R^2 = 0.036). (**F**) Cross-sectional analysis of frequency (% of $CD19^+$ $CD20^+$ B cells) of SARS-CoV-2 RBD-specific IgM^+ memory B cells. Second order polynomial model for best fit curve (R^2 = 0.034). (**G**) Cross-sectional analysis of frequency (% of $CD19^+$ $CD20^+$ B cells) of SARS-CoV-2 nucleocapsid-specific IgA^+ memory B cells. Second order polynomial model for best fit curve (R^2 = 0.0031). (**H**) Cross-sectional analysis of frequency (% of $CD19^+$ $CD20^+$ B cells) of SARS-CoV-2 nucleocapsid-specific IgM^+ memory B cells. Second order polynomial model for best fit curve (R^2 = 0.029). (**I**) Cross-sectional analysis of geometric mean fluorescence intensity of spike, RBD and nucleocapsid probes on S-, RBD- and nucleocapsid-specific memory B cells, respectively. Data shown are simple linear-regression lines for individual probes. (**J**) Cross-sectional analysis of geometric mean fluorescence intensity of spike, RBD and nucleocapsid probes on S-, RBD- and nucleocapsid-specific memory B cells, respectively, normalized to a positive control sample. Data shown are simple linear-regression lines for individual antigen.

Figure S3. SARS-CoV-2 circulating memory $CD8^+$ T cells. (A) Gating strategies to define SARS-CoV-2-specific $CD8^+$ T cells by AIM assay, using individual SARS-CoV-2 ORF peptide pools. **(B)** Representative examples of flow cytometry plots of SARS-CoV-2-specific $CD8^+$ T cells ($CD69^+$ $CD137^+$, after overnight stimulation with S, M, N, ORF3a, or nsp3 peptide pools, compared to negative control (DMSO) from three COVID-19 subjects and one uninfected control. **(C)** Cross-sectional analysis of total SARS-CoV-2-specific $CD4^+$ T cells, as per Figure 3, but graphing stimulation index (SI). n = 155 COVID-19 subject samples (clear circles) for cross-sectional analysis. n = 30 COVID-19 subjects (white circles) for longitudinal analysis.

Figure S4. SARS-CoV-2 circulating memory $CD4^+$ T cells. (A) Gating strategies to define SARS-CoV-2-specific $CD4^+$ T cells by AIM assay, using individual SARS-CoV-2 ORF peptide pools. **(B)** Representative examples of flow cytometry plots of SARS-CoV-2-specific $CD4^+$ T cells ($OX40^+$ $CD137^+$, after overnight stimulation with S, M, N, ORF3a, or nsp3 peptide pools, compared to negative control (DMSO). From three COVID-19 subjects and one uninfected control. **(C)** Cross-sectional analysis of total SARS-CoV-2-specific $CD4^+$ T cells, as per Figure 4, but graphing stimulation index (SI). **(D)** Cross-sectional analysis of M-specific $CD4^+$ T cells. **(E)** Longitudinal analysis of M-specific $CD4^+$ T cells in paired samples from the same subjects. n = 155 COVID-19 subject samples (white circles) for cross-sectional analysis. n = 30 COVID-19 subjects (white circles) for longitudinal analysis.

Figure S5. SARS-CoV-2 memory T_{FH} cells. (A) Gating strategies to define SARS-CoV-2-specific $CD4^+$ T cells by AIM assay, using S and MP_R peptide pools. **(B)** Representative examples of flow cytometry plots

of SARS-CoV-2-specific $CD4^+$ T cells. Surface $CD40L^+$ $OX40^+$, after overnight stimulation with S and MP_R peptide pools, compared to negative control (DMSO) from a representative COVID-19 subject and an uninfected control. **(C, D)** SARS-CoV-2-specific $CD4^+$ T cells based on surface $CD40L^+$ $OX40^+$, gated as in A, after overnight stimulation with S or MP_R peptide pools. n = 34 COVID-19 subject samples (white circles), n = 21 at 1-2 mo, n = 13 at 6 mo. The dotted black line indicates LOD.* $p<0.05$, **$p<0.01$, *** $p<0.001$, **** $p<0.0001$.

Figure S6. Immune memory and disease severity. (A) Spike IgG, as per Figure 1. Symbol colors represent disease severity (white: asymptomatic, gray: mild, black: moderate, red: severe). **(B)** Cross-sectional analysis of SARS-CoV-2 spike-specific total (IgG^+, IgA^+, or IgA^+) memory B cells, as per Figure 2C, color coded based on subject COVID-19 disease severity. **(C)** Cross-sectional analysis of SARS-CoV-2 RBD-specific total (IgG^+, IgA^+, or IgA^+) memory B cells, as per Figure 2E, color coded based on subject COVID-19 disease severity. **(D)** Cross-sectional analysis of SARS-CoV-2 nucleocapsid-specific total (IgG^+, IgA^+, or IgA^+) memory B cells, as per Figure 2F, color coded based on subject COVID-19 disease severity. **(E)** Cross-sectional analysis of SARS-CoV-2-specific $CD8^+$ T cells, as per Figure 3B, color coded based on subject COVID-19 disease severity. **(F)** Cross-sectional analysis of SARS-CoV-2-specific $CD4^+$ T cells, as per Figure 4B, color coded based on subject COVID-19 disease severity.

Figure S7. Immune memory and gender. Cross-sectional analyses of SARS-CoV-2 serologies by male and female gender. **(A)** Nucleocapsid IgG titers. Males: Linear decay preferred model, $t_{1/2}$ = 69d, 95% CI: 42-209d, R = -0.28, p=0.0035. Females: linear decay preferred model, $t_{1/2}$ = 64d, 95% CI: 47-104d, R = -0.41, p<0.0001. **(B)** RBD IgG titers. Males: One phase decay preferred model, $t_{1/2}$ = 24d, 95% CI 10-122d, R = -0.38, p<0.0001. Females: linear decay preferred model, $t_{1/2}$ = 94d,95% CI: 64-179d R = -0.34, p=0.0.0002. **(C)** RBD IgA titers. Males: One phase decay preferred model, $t_{1/2}$ = 15d,95% CI 8-30d, R = -0.45, p<0.0001. Females: linear decay preferred model, $t_{1/2}$ = 92d, 95% CI: 60-195d, R = -0.32, p=0.0004. **(D)** Pseudovirus neutralizing titers. Males: One phase decay preferred model, $t_{1/2}$ = 16d, 95% CI: 7-49d, R = -0.35, p=0.0022. Females: linear decay preferred model, $t_{1/2}$ = 169d, 95% CI: 96-710d, R = -0.25, p=0.0069. **(E)** Spike IgA titers. Males: One phase decay preferred model, $t_{1/2}$ = 8d, 95% CI 4-13d, R = -0.22, p=0.019. Females: linear decay preferred model, $t_{1/2}$ = 337d, 95% CI 116-370d: R = -0.056, p=0.54. **(F)** Cross-sectional analysis of frequency (% of $CD19^+$ $CD20^+$ B cells) of SARS-CoV-2 spike-specific memory B cells (IgG^+, IgA^+, or IgM^+), as per Figure 2C, color coded based on subject gender Pseudo-first order kinetic model for best fit curves. R^2 = 0.27 (females), R^2 = 0.057 (males). No significant difference between males and females. p = 0.10 by One-way ANCOVA. **(G)** Cross-sectional analysis of SARS-CoV-2 RBD-specific total (IgG^+, IgA^+, or IgA^+) memory B cells, as per Figure 2E, color coded based on subject gender. Second order polynomial model for best fit curves. R^2 = 0.37 (females) and R^2 = 0.12 (males). No significant difference between males and females. p = 0.24 by one-way ANCOVA. **(H)** Cross-sectional analysis of SARS-CoV-2 nucleocapsid-specific total (IgG^+, IgA^+, or IgA^+) memory B cells, as per Figure 2F, color coded based on subject gender. Second order polynomial model for best fit curves. R^2 = 0.28 (females), R^2 = 0.16 (males). No significant difference between males and females. p = 0.45 by one-way ANCOVA. **(I)**. No significant difference between males and females. p = 0.16 by one-way ANCOVA. **(J)** No significant difference between males and females. p = 0.24 by one-way ANCOVA.

Figure S8. Immune memory relationships. (A) The ratio of SARS-CoV-2 specific $CD4^+$ T cell frequency relative to SARS-CoV-2 specific $CD8^+$ T cell frequency (best-fit simple linear regression line, R^2 = 0.02932). Two data points are outside the axis limits. **(B)** The ratio of RBD-specific memory B cell frequency (percentage) relative to RBD-specific IgG (pseudo-first order kinetic model, R^2 = 0.3659).

Three data points are outside the axis limits **(C)** The ratio of RBD-specific memory B cell frequency (percentage) relative to RBD IgA antibodies (pseudo-first order kinetic model, R^2 = 0.3804). Two data points are outside the axis limits. **(D)** The ratio of SARS-CoV-2 specific $CD4^+$ T cell frequency relative to RBD IgG antibodies (best-fit simple linear regression line, R^2 = 0.0003891). Two data points are outside the axis limits. **(E)** The ratio of RBD-specific memory B cell frequency (percentage) relative to total SARS-CoV-2 specific $CD4^+$ T cell frequency (best-fit simple linear regression line, R^2 = 0.2351). One data point is outside the axis limits. For Figure 5: The ratio of RBD-specific memory B cell frequency (percentage) relative to RBD IgA antibodies (orange curve; best-fit second order polynomial curve transformed by $\times 10^5$), RBD IgG antibodies (magenta; best-fit simple linear regression line transformed by $\times 10^5$) and total SARS-CoV-2 specific $CD4^+$ T cell frequency (blue; best-fit simple linear regression line transformed by $\times 10^2$), or the ratio of SARS-CoV-2 specific $CD4^+$ T cell frequency relative to SARS-CoV-2 specific $CD8^+$ T cell frequency (till; best-fit simple linear regression line) and RBD IgG antibodies (black; best-fit simple linear regression line transformed by $\times 10^3$).

REFERENCES

1. D. S. Stephens, M. J. McElrath, COVID-19 and the Path to Immunity. *Jama*. **324** (2020), doi:10.1001/jama.2020.16656.
2. A. Grifoni, D. Weiskopf, S. I. Ramirez, J. Mateus, J. M. Dan, C. R. Moderbacher, S. A. Rawlings, A. Sutherland, L. Premkumar, R. S. Jadi, D. Marrama, A. M. de Silva, A. Frazier, A. Carlin, J. A. Greenbaum, B. Peters, F. Krammer, D. M. Smith, S. Crotty, A. Sette, Targets of T cell responses to SARS-CoV-2 coronavirus in humans with COVID-19 disease and unexposed individuals. *Cell*. **181**, 1489-1501.e15 (2020).
3. F. Krammer, SARS-CoV-2 vaccines in development. *Nature*, 1–16 (2020).
4. M. S. Suthar, M. G. Zimmerman, R. C. Kauffman, G. Mantus, S. L. Linderman, W. H. Hudson, A. Vanderheiden, L. Nyhoff, C. W. Davis, S. Adekunle, M. Affer, M. Sherman, S. Reynolds, H. P. Verkerke, D. N. Alter, J. Guarner, J. Bryksin, M. Horwath, C. M. Arthur, N. Saakadze, G. H. Smith, S. Edupuganti, E. M. Scherer, K. Hellmeister, A. Cheng, J. A. Morales, A. S. Neish, S. R. Stowell, F. Frank, E. Ortlund, E. Anderson, V. D. Menachery, N. Rouphael, A. Mehta, D. S. Stephens, R. Ahmed, J. D. Roback, J. Wrammert, Rapid generation of neutralizing antibody responses in COVID-19 patients. *Cell Reports Medicine*. **1**, 100040 (2020).
5. C. R. Moderbacher, S. I. Ramirez, J. M. Dan, A. Grifoni, K. M. Hastie, D. Weiskopf, S. Belanger, R. K. Abbott, C. Kim, J. Choi, Y. Kato, E. G. Crotty, C. Kim, S. A. Rawlings, J. Mateus, L. P. V. Tse, A. Frazier, R. Baric, B. Peters, J. Greenbaum, E. O. Saphire, D. M. Smith, A. Sette, S. Crotty, Antigen-specific adaptive immunity to SARS-CoV-2 in acute COVID-19 and associations with age and disease severity. *Cell* (2020), doi:10.1016/j.cell.2020.09.038.
6. R. Zhou, K. K.-W. To, Y.-C. Wong, L. Liu, B. Zhou, X. Li, H. Huang, Y. Mo, T.-Y. Luk, T. T.-K. Lau, P. Yeung, W.-M. Chan, A. K.-L. Wu, K.-C. Lung, O. T.-Y. Tsang, W.-S. Leung, I. F.-N. Hung, K.-Y. Yuen, Z. Chen, Acute SARS-CoV-2 infection impairs dendritic cell and T cell responses. *Immunity* (2020), doi:10.1016/j.immuni.2020.07.026.
7. M. Liao, Y. Liu, J. Yuan, Y. Wen, G. Xu, J. Zhao, L. Cheng, J. Li, X. Wang, F. Wang, L. Liu, I. Amit, S. Zhang, Z. Zhang, Single-cell landscape of bronchoalveolar immune cells in patients with COVID-19. *Nat Med*. **26**, 842–844 (2020).
8. A. G. Laing, A. Lorenc, I. del M. del Barrio, A. Das, M. Fish, L. Monin, M. Muñoz-Ruiz, D. R. McKenzie, T. S. Hayday, I. Francos-Quijorna, S. Kamdar, M. Joseph, D. Davies, R. Davis, A. Jennings, I. Zlatareva, P. Vantourout, Y. Wu, V. Sofra, F. Cano, M. Greco, E. Theodoridis, J. Freedman, S. Gee, J. N. E. Chan, S. Ryan, E. Bugallo-Blanco, P. Peterson, K. Kisand, L. Haljasmägi, L. Chadli, P. Moingeon, L. Martinez, B. Merrick, K. Bisnauthsing, K. Brooks, M. A. A. Ibrahim, J. Mason, F. L. Gomez, K. Babalola, S. Abdul-Jawad, J. Cason, C. Mant, J. Seow, C. Graham, K. J. Doores, F. D. Rosa, J. Edgeworth, M. Shankar-Hari, A. C. Hayday, A dynamic COVID-19 immune signature includes associations with poor prognosis. *Nat Med*, 1–13 (2020).
9. D. Blanco-Melo, B. E. Nilsson-Payant, W.-C. Liu, S. Uhl, D. Hoagland, R. Møller, T. X. Jordan, K. Oishi, M. Panis, D. Sachs, T. T. Wang, R. E. Schwartz, J. K. Lim, R. A. Albrecht, B. R. tenOever, Imbalanced Host Response to SARS-CoV-2 Drives Development of COVID-19. *Cell*. **181**, 1036-1045.e9 (2020).
10. P. S. Arunachalam, F. Wimmers, C. K. P. Mok, R. A. P. M. Perera, M. Scott, T. Hagan, N. Sigal, Y. Feng, L. Bristow, O. T.-Y. Tsang, D. Wagh, J. Coller, K. L. Pellegrini, D. Kazmin, G. Alaaeddine, W. S. Leung, J. M. C. Chan, T. S. H. Chik, C. Y. C. Choi, C. Huerta, M. P. McCullough, H. Lv, E. Anderson, S. Edupuganti, A. A. Upadhyay, S. E. Bosinger, H. T. Maecker, P. Khatri, N. Rouphael, M. Peiris, B. Pulendran, Systems biological assessment of immunity to mild versus severe COVID-19 infection in humans. *Science*, eabc6261 (2020).

11. P. Bastard, L. B. Rosen, Q. Zhang, E. Michailidis, H.-H. Hoffmann, Y. Zhang, K. Dorgham, Q. Philippot, J. Rosain, V. Béziat, J. Manry, E. Shaw, L. Haljasmägi, P. Peterson, L. Lorenzo, L. Bizien, S. Trouillet-Assant, K. Dobbs, A. A. de Jesus, A. Belot, A. Kallaste, E. Catherinot, Y. Tandjaoui-Lambiotte, J. L. Pen, G. Kerner, B. Bigio, Y. Seeleuthner, R. Yang, A. Bolze, A. N. Spaan, O. M. Delmonte, M. S. Abers, A. Aiuti, G. Casari, V. Lampasona, L. Piemonti, F. Ciceri, K. Bilguvar, R. P. Lifton, M. Vasse, D. M. Smadja, M. Migaud, J. Hadjadj, B. Terrier, D. Duffy, L. Quintana-Murci, D. van de Beek, L. Roussel, D. C. Vinh, S. G. Tangye, F. Haerynck, D. Dalmau, J. Martinez-Picado, P. Brodin, M. C. Nussenzweig, S. Boisson-Dupuis, C. Rodríguez-Gallego, G. Vogt, T. H. Mogensen, A. J. Oler, J. Gu, P. D. Burbelo, J. Cohen, A. Biondi, L. R. Bettini, M. D'Angio, P. Bonfanti, P. Rossignol, J. Mayaux, F. Rieux-Laucat, E. S. Husebye, F. Fusco, M. V. Ursini, L. Imberti, A. Sottini, S. Paghera, E. Quiros-Roldan, C. Rossi, R. Castagnoli, D. Montagna, A. Licari, G. L. Marseglia, X. Duval, J. Ghosn, H. Lab§, N.-U. I. R. to C. Group§, C. Clinicians§, C.-S. Clinicians§, I. C. Group§, F. C. C. S. Group§, T. M. I. Consortium§, C.-C. Cohort§, A. U. C.-19 Biobank§, C. H. G. Effort§, J. S. Tsang, R. Goldbach-Mansky, K. Kisand, M. S. Lionakis, A. Puel, S.-Y. Zhang, S. M. Holland, G. Gorochov, E. Jouanguy, C. M. Rice, A. Cobat, L. D. Notarangelo, L. Abel, H. C. Su, J.-L. Casanova, Auto-antibodies against type I IFNs in patients with life-threatening COVID-19. *Science*, eabd4585 (2020).
12. Q. Zhang, P. Bastard, Z. Liu, J. L. Pen, M. Moncada-Velez, J. Chen, M. Ogishi, I. K. D. Sabli, S. Hodeib, C. Korol, J. Rosain, K. Bilguvar, J. Ye, A. Bolze, B. Bigio, R. Yang, A. A. Arias, Q. Zhou, Y. Zhang, F. Onodi, S. Korniotis, L. Karpf, Q. Philippot, M. Chbihi, L. Bonnet-Madin, K. Dorgham, N. Smith, W. M. Schneider, B. S. Razooky, H.-H. Hoffmann, E. Michailidis, L. Moens, J. E. Han, L. Lorenzo, L. Bizien, P. Meade, A.-L. Neehus, A. C. Ugurbil, A. Corneau, G. Kerner, P. Zhang, F. Rapaport, Y. Seeleuthner, J. Manry, C. Masson, Y. Schmitt, A. Schlüter, T. L. Voyer, T. Khan, J. Li, J. Fellay, L. Roussel, M. Shahrooei, M. F. Alosaimi, D. Mansouri, H. Al-Saud, F. Al-Mulla, F. Almourfi, S. Z. Al-Muhsen, F. Alsohime, S. A. Turki, R. Hasanato, D. van de Beek, A. Biondi, L. R. Bettini, M. D'Angio, P. Bonfanti, L. Imberti, A. Sottini, S. Paghera, E. Quiros-Roldan, C. Rossi, A. J. Oler, M. F. Tompkins, C. Alba, I. Vandernoot, J.-C. Goffard, G. Smits, I. Migeotte, F. Haerynck, P. Soler-Palacin, A. Martin-Nalda, R. Colobran, P.-E. Morange, S. Keles, F. Çölkesen, T. Ozcelik, K. K. Yasar, S. Senoglu, Ş. N. Karabela, C. R. Gallego, G. Novelli, S. Hraiech, Y. Tandjaoui-Lambiotte, X. Duval, C. Laouénan, C.-S. Clinicians†, C. Clinicians†, I. C. Group†, F. C. C. S. Group†, C.-C. Cohort†, A. U. Covid-19, Biobank†, C. H. G. Effort†, NIAID-USUHS, T. C. I. Group†, A. L. Snow, C. L. Dalgard, J. Milner, D. C. Vinh, T. H. Mogensen, N. Marr, A. N. Spaan, B. Boisson, S. Boisson-Dupuis, J. Bustamante, A. Puel, M. Ciancanelli, I. Meyts, T. Maniatis, V. Soumelis, A. Amara, M. Nussenzweig, A. García-Sastre, F. Krammer, A. Pujol, D. Duffy, R. Lifton, S.-Y. Zhang, G. Gorochov, V. Béziat, E. Jouanguy, V. Sancho-Shimizu, C. M. Rice, L. Abel, L. D. Notarangelo, A. Cobat, H. C. Su, J.-L. Casanova, Inborn errors of type I IFN immunity in patients with life-threatening COVID-19. *Science*, eabd4570 (2020).
13. D. M. D. Valle, S. Kim-Schulze, H.-H. Huang, N. D. Beckmann, S. Nirenberg, B. Wang, Y. Lavin, T. H. Swartz, D. Madduri, A. Stock, T. U. Marron, H. Xie, M. Patel, K. Tuballes, O. V. Oekelen, A. Rahman, P. Kovatch, J. A. Aberg, E. Schadt, S. Jagannath, M. Mazumdar, A. W. Charney, A. Firpo-Betancourt, D. R. Mendu, J. Jhang, D. Reich, K. Sigel, C. Cordon-Cardo, M. Feldmann, S. Parekh, M. Merad, S. Gnjatic, An inflammatory cytokine signature predicts COVID-19 severity and survival. *Nat Med*, 1–8 (2020).
14. L. Kuri-Cervantes, M. B. Pampena, W. Meng, A. M. Rosenfeld, C. A. G. Ittner, A. R. Weisman, R. S. Agyekum, D. Mathew, A. E. Baxter, L. A. Vella, O. Kuthuru, S. A. Apostolidis, L. Bershaw, J. Dougherty, A. R. Greenplate, A. Pattekar, J. Kim, N. Han, S. Gouma, M. E. Weirick, C. P. Arevalo, M. J. Bolton, E. C. Goodwin, E. M. Anderson, S. E. Hensley, T. K. Jones, N. S. Mangalmurti, E. T. L. Prak, E. J. Wherry, N. J. Meyer, M. R. Betts, Comprehensive mapping of immune perturbations associated with severe COVID-19. *Sci Immunol*. **5**, eabd7114 (2020).

15. S. Li, L. Jiang, X. Li, F. Lin, Y. Wang, B. Li, T. Jiang, W. An, S. Liu, H. Liu, P. Xu, L. Zhao, L. Zhang, J. Mu, H. Wang, J. Kang, Y. Li, L. Huang, C. Zhu, S. Zhao, J. Lu, J. Ji, J. Zhao, Clinical and pathological investigation of severe COVID-19 patients. *Jci Insight*. **5** (2020), doi:10.1172/jci.insight.138070.
16. C. Radermecker, N. Detrembleur, J. Guiot, E. Cavalier, M. Henket, C. d'Emal, C. Vanwinge, D. Cataldo, C. Oury, P. Delvenne, T. Marichal, Neutrophil extracellular traps infiltrate the lung airway, interstitial, and vascular compartments in severe COVID-19. *J Exp Med*. **217** (2020), doi:10.1084/jem.20201012.
17. B. Schurink, E. Roos, T. Radonic, E. Barbe, C. S. C. Bouman, H. H. de Boer, G. J. de Bree, E. B. Bulle, E. M. Aronica, S. Florquin, J. Fronczek, L. M. A. Heunks, M. D. de Jong, L. Guo, R. du Long, R. Lutter, P. C. G. Molenaar, E. A. Neefjes-Borst, H. W. M. Niessen, C. J. M. van Noesel, J. J. T. H. Roelofs, E. J. Snijder, E. C. Soer, J. Verheij, A. P. J. Vlaar, W. Vos, N. N. van der Wel, A. C. van der Wal, P. van der Valk, M. Bugiani, Viral presence and immunopathology in patients with lethal COVID-19: a prospective autopsy cohort study. *Lancet Microbe* (2020), doi:10.1016/s2666-5247(20)30144-0.
18. M. Aid, K. Busman-Sahay, S. J. Vidal, Z. Maliga, S. Bondoc, C. Starke, M. Terry, C. A. Jacobson, L. Wrijil, S. Ducat, O. R. Brook, A. D. Miller, M. Porto, K. L. Pellegrini, M. Pino, T. N. Hoang, A. Chandrashekar, S. Patel, K. Stephenson, S. E. Bosinger, H. Andersen, M. G. Lewis, J. L. Hecht, P. K. Sorger, A. J. Martinot, J. D. Estes, D. H. Barouch, Vascular Disease and Thrombosis in SARS-CoV-2 Infected Rhesus Macaques. *Cell* (2020), doi:10.1016/j.cell.2020.10.005.
19. N. Baumgarth, J. Nikolich-Žugich, F. E.-H. Lee, D. Bhattacharya, Antibody Responses to SARS-CoV-2: Let's Stick to Known Knowns. *J Immunol*, ji2000839 (2020).
20. A. Wajnberg, F. Amanat, A. Firpo, D. Altman, M. Bailey, M. Mansour, M. McMahon, P. Meade, D. R. Mendu, K. Muellers, D. Stadlbauer, K. Stone, S. Strohmeier, J. Aberg, D. Reich, F. Krammer, C. Cordon-Cardo, SARS-CoV-2 infection induces robust, neutralizing antibody responses that are stable for at least three months (n.d.), doi:10.1101/2020.07.14.20151126.
21. A. Sariol, S. Perlman, Lessons for COVID-19 immunity from other coronavirus infections. *Immunity*. **53**, 248–263 (2020).
22. K. Subbarao, SARS-CoV-2: A New Song Recalls an Old Melody. *Cell Host Microbe*. **27**, 692–694 (2020).
23. W. Deng, L. Bao, J. Liu, C. Xiao, J. Liu, J. Xue, Q. Lv, F. Qi, H. Gao, P. Yu, Y. Xu, Y. Qu, F. Li, Z. Xiang, H. Yu, S. Gong, M. Liu, G. Wang, S. Wang, Z. Song, Y. Liu, W. Zhao, Y. Han, L. Zhao, X. Liu, Q. Wei, C. Qin, Primary exposure to SARS-CoV-2 protects against reinfection in rhesus macaques. *Science*, eabc5343 (2020).
24. Q. Gao, L. Bao, H. Mao, L. Wang, K. Xu, M. Yang, Y. Li, L. Zhu, N. Wang, Z. Lv, H. Gao, X. Ge, B. Kan, Y. Hu, J. Liu, F. Cai, D. Jiang, Y. Yin, C. Qin, J. Li, X. Gong, X. Lou, W. Shi, D. Wu, H. Zhang, L. Zhu, W. Deng, Y. Li, J. Lu, C. Li, X. Wang, W. Yin, Y. Zhang, C. Qin, Rapid development of an inactivated vaccine candidate for SARS-CoV-2. *Science*, eabc1932 (2020).
25. A. Chandrashekar, J. Liu, A. J. Martinot, K. McMahan, N. B. Mercado, L. Peter, L. H. Tostanoski, J. Yu, Z. Maliga, M. Nekorchuk, K. Busman-Sahay, M. Terry, L. M. Wrijil, S. Ducat, D. R. Martinez, C. Atyeo, S. Fischinger, J. S. Burke, M. D. Slein, L. Pessaint, A. V. Ry, J. Greenhouse, T. Taylor, K. Blade, A. Cook, B. Finneyfrock, R. Brown, E. Teow, J. Velasco, R. Zahn, F. Wegmann, P. Abbink, E. A. Bondzie, G. Dagotto, M. S. Gebre, X. He, C. Jacob-Dolan, N. Kordana, Z. Li, M. A. Lifton, S. H. Mahrokhian, L. F. Maxfield, R. Nityanandam, J. P. Nkolola, A. G. Schmidt, A. D. Miller, R. S. Baric, G. Alter, P. K. Sorger, J. D. Estes, H. Andersen, M. G. Lewis, D. H. Barouch, SARS-CoV-2 infection protects against rechallenge in rhesus macaques. *Science*, eabc4776 (2020).
26. A. Addetia, K. H. D. Crawford, A. Dingens, H. Zhu, P. Roychoudhury, M.-L. Huang, K. R. Jerome, J. D. Bloom, A. L. Greninger, Neutralizing antibodies correlate with protection from SARS-CoV-2 in

humans during a fishery vessel outbreak with high attack rate. *J Clin Microbiol* (2020), doi:10.1128/jcm.02107-20.
27. S. J. Zost, P. Gilchuk, J. B. Case, E. Binshtein, R. E. Chen, J. P. Nkolola, A. Schäfer, J. X. Reidy, A. Trivette, R. S. Nargi, R. E. Sutton, N. Suryadevara, D. R. Martinez, L. E. Williamson, E. C. Chen, T. Jones, S. Day, L. Myers, A. O. Hassan, N. M. Kafai, E. S. Winkler, J. M. Fox, S. Shrihari, B. K. Mueller, J. Meiler, A. Chandrashekar, N. B. Mercado, J. J. Steinhardt, K. Ren, Y.-M. Loo, N. L. Kallewaard, B. T. McCune, S. P. Keeler, M. J. Holtzman, D. H. Barouch, L. E. Gralinski, R. S. Baric, L. B. Thackray, M. S. Diamond, R. H. Carnahan, J. E. Crowe, Potently neutralizing and protective human antibodies against SARS-CoV-2. *Nature*, 1–10 (2020).
28. T. F. Rogers, F. Zhao, D. Huang, N. Beutler, A. Burns, W. He, O. Limbo, C. Smith, G. Song, J. Woehl, L. Yang, R. K. Abbott, S. Callaghan, E. Garcia, J. Hurtado, M. Parren, L. Peng, S. Ramirez, J. Ricketts, M. J. Ricciardi, S. A. Rawlings, N. C. Wu, M. Yuan, D. M. Smith, D. Nemazee, J. R. Teijaro, J. E. Voss, I. A. Wilson, R. Andrabi, B. Briney, E. Landais, D. Sok, J. G. Jardine, D. R. Burton, Isolation of potent SARS-CoV-2 neutralizing antibodies and protection from disease in a small animal model. *Science*, eabc7520 (2020).
29. A. Baum, R. Copin, D. Ajithdoss, A. Zhou, K. Lanza, N. Negron, M. Ni, Y. Wei, G. S. Atwal, A. Oyejide, Y. Goez-Gazi, J. Dutton, E. Clemmons, H. M. Staples, C. Bartley, B. Klaffke, K. Alfson, M. Gazi, O. Gonzales, E. Dick, R. Carrion, L. Pessaint, M. Porto, A. Cook, R. Brown, V. Ali, J. Greenhouse, T. Taylor, H. Andersen, M. G. Lewis, N. Stahl, A. J. Murphy, G. D. Yancopoulos, C. A. Kyratsous, *Biorxiv*, in press, doi:10.1101/2020.08.02.233320.
30. Regeneron, REGN-COV2 ANTIBODY COCKTAIL PROGRAM UPDATE (n.d.), (available at https://newsroom.regeneron.com/static-files/a596a85e-e72d-4529-8eb5-d52d87a99070).
31. Lilly announces proof of concept data for neutralizing antibody LY-CoV555 in the COVID-19 outpatient setting | Eli Lilly and Company (n.d.), (available at https://investor.lilly.com/news-releases/news-release-details/lilly-announces-proof-concept-data-neutralizing-antibody-ly).
32. D. M. Altmann, R. J. Boyton, SARS-CoV-2 T cell immunity: Specificity, function, durability, and role in protection. *Sci Immunol*. **5**, eabd6160 (2020).
33. P. V. Damme, K. V. Herck, A review of the long-term protection after hepatitis A and B vaccination. *Travel Med Infect Di*. **5**, 79–84 (2007).
34. M. M. Rosado, M. Scarsella, E. Pandolfi, S. Cascioli, E. Giorda, P. Chionne, E. Madonne, F. Gesualdo, M. Romano, C. M. Ausiello, M. Rapicetta, A. R. Zanetti, A. Tozzi, R. Carsetti, Switched memory B cells maintain specific memory independently of serum antibodies: The hepatitis B example. *Eur J Immunol*. **41**, 1800–1808 (2011).
35. F. Zhou, T. Yu, R. Du, G. Fan, Y. Liu, Z. Liu, J. Xiang, Y. Wang, B. Song, X. Gu, L. Guan, Y. Wei, H. Li, X. Wu, J. Xu, S. Tu, Y. Zhang, H. Chen, B. Cao, Clinical course and risk factors for mortality of adult inpatients with COVID-19 in Wuhan, China: a retrospective cohort study. *Lancet*. **395**, 1054–1062 (2020).
36. W. A. Orenstein, R. Ahmed, Simply put: Vaccination saves lives. *Proc National Acad Sci*. **114**, 4031–4033 (2017).
37. P. Piot, H. J. Larson, K. L. O'Brien, J. N'kengasong, E. Ng, S. Sow, B. Kampmann, Immunization: vital progress, unfinished agenda. *Nature*. **575**, 119–129 (2019).
38. S. Plotkin, W. Orenstein, P. Offit, *Plotkin's vaccines, 7th edition* (Elsevier, 2018), *Elsevier*.
39. F. Sallusto, A. Lanzavecchia, K. Araki, R. Ahmed, From vaccines to memory and back. *Immunity*. **33**, 451–463 (2010).
40. S. Crotty, R. Ahmed, Immunological memory in humans. *Seminars in Immunology*. **16**, 197–203 (2004).

41. F. Weisel, M. Shlomchik, Memory B Cells of Mice and Humans. *Annual review of immunology*. **35**, 255–284 (2017).
42. S. M. Kissler, C. Tedijanto, E. Goldstein, Y. H. Grad, M. Lipsitch, Projecting the transmission dynamics of SARS-CoV-2 through the postpandemic period. *Science*. **368**, 860–868 (2020).
43. C. M. Saad-Roy, C. E. Wagner, R. E. Baker, S. E. Morris, J. Farrar, A. L. Graham, S. A. Levin, M. J. Mina, C. J. E. Metcalf, B. T. Grenfell, Immune life history, vaccination, and the dynamics of SARS-CoV-2 over the next 5 years. *Science*, eabd7343 (2020).
44. L. B. Rodda, J. Netland, L. Shehata, K. B. Pruner, P. M. Morawski, C. Thouvenel, K. K. Takehara, J. Eggenberger, E. A. Hemann, H. R. Waterman, M. L. Fahning, Y. Chen, J. Rathe, C. Stokes, S. Wrenn, B. Fiala, L. P. Carter, J. A. Hamerman, N. P. King, M. Gale, D. J. Campbell, D. Rawlings, M. Pepper, Functional SARS-CoV-2-specific immune memory persists after mild COVID-19. *Medrxiv Prepr Serv Heal Sci* (2020), doi:10.1101/2020.08.11.20171843.
45. Q.-X. Long, X.-J. Tang, Q.-L. Shi, Q. Li, H.-J. Deng, J. Yuan, J.-L. Hu, W. Xu, Y. Zhang, F.-J. Lv, K. Su, F. Zhang, J. Gong, B. Wu, X.-M. Liu, J.-J. Li, J.-F. Qiu, J. Chen, A.-L. Huang, Clinical and immunological assessment of asymptomatic SARS-CoV-2 infections. *Nat Med*. **26**, 1200–1204 (2020).
46. D. F. Gudbjartsson, G. L. Norddahl, P. Melsted, K. Gunnarsdottir, H. Holm, E. Eythorsson, A. O. Arnthorsson, D. Helgason, K. Bjarnadottir, R. F. Ingvarsson, B. Thorsteinsdottir, S. Kristjansdottir, K. Birgisdottir, A. M. Kristinsdottir, M. I. Sigurdsson, G. A. Arnadottir, E. V. Ivarsdottir, M. Andresdottir, F. Jonsson, A. B. Agustsdottir, J. Berglund, B. Eiriksdottir, R. Fridriksdottir, E. E. Gardarsdottir, M. Gottfredsson, O. S. Gretarsdottir, S. Gudmundsdottir, K. R. Gudmundsson, T. R. Gunnarsdottir, A. Gylfason, A. Helgason, B. O. Jensson, A. Jonasdottir, H. Jonsson, T. Kristjansson, K. G. Kristinsson, D. N. Magnusdottir, O. T. Magnusson, L. B. Olafsdottir, S. Rognvaldsson, L. le Roux, G. Sigmundsdottir, A. Sigurdsson, G. Sveinbjornsson, K. E. Sveinsdottir, M. Sveinsdottir, E. A. Thorarensen, B. Thorbjornsson, M. Thordardottir, J. Saemundsdottir, S. H. Kristjansson, K. S. Josefsdottir, G. Masson, G. Georgsson, M. Kristjansson, A. Moller, R. Palsson, T. Gudnason, U. Thorsteinsdottir, I. Jonsdottir, P. Sulem, K. Stefansson, Humoral Immune Response to SARS-CoV-2 in Iceland. *New Engl J Med* (2020), doi:10.1056/nejmoa2026116.
47. L. Piccoli, Y.-J. Park, M. A. Tortorici, N. Czudnochowski, A. C. Walls, M. Beltramello, C. Silacci-Fregni, D. Pinto, L. E. Rosen, J. E. Bowen, O. J. Acton, S. Jaconi, B. Guarino, A. Minola, F. Zatta, N. Sprugasci, J. Bassi, A. Peter, A. D. Marco, J. C. Nix, F. Mele, S. Jovic, B. F. Rodriguez, S. V. Gupta, F. Jin, G. Piumatti, G. L. Presti, A. F. Pellanda, M. Biggiogero, M. Tarkowski, M. S. Pizzuto, E. Cameroni, C. Havenar-Daughton, M. Smithey, D. Hong, V. Lepori, E. Albanese, A. Ceschi, E. Bernasconi, L. Elzi, P. Ferrari, C. Garzoni, A. Riva, G. Snell, F. Sallusto, K. Fink, H. W. Virgin, A. Lanzavecchia, D. Corti, D. Veesler, Mapping neutralizing and immunodominant sites on the SARS-CoV-2 spike receptor-binding domain by structure-guided high-resolution serology. *Cell* (2020), doi:10.1016/j.cell.2020.09.037.
48. D. F. Robbiani, C. Gaebler, F. Muecksch, J. C. C. Lorenzi, Z. Wang, A. Cho, M. Agudelo, C. O. Barnes, A. Gazumyan, S. Finkin, T. Hägglöf, T. Y. Oliveira, C. Viant, A. Hurley, H.-H. Hoffmann, K. G. Millard, R. G. Kost, M. Cipolla, K. Gordon, F. Bianchini, S. T. Chen, V. Ramos, R. Patel, J. Dizon, I. Shimeliovich, P. Mendoza, H. Hartweger, L. Nogueira, M. Pack, J. Horowitz, F. Schmidt, Y. Weisblum, E. Michailidis, A. W. Ashbrook, E. Waltari, J. E. Pak, K. E. Huey-Tubman, N. Koranda, P. R. Hoffman, A. P. West, C. M. Rice, T. Hatziioannou, P. J. Bjorkman, P. D. Bieniasz, M. Caskey, M. C. Nussenzweig, Convergent antibody responses to SARS-CoV-2 in convalescent individuals. *Nature*, 1–8 (2020).
49. J. Yu, L. H. Tostanoski, L. Peter, N. B. Mercado, K. McMahan, S. H. Mahrokhian, J. P. Nkolola, J. Liu, Z. Li, A. Chandrashekar, D. R. Martinez, C. Loos, C. Atyeo, S. Fischinger, J. S. Burke, M. D. Slein, Y. Chen, A. Zuiani, F. J. N. Lelis, M. Travers, S. Habibi, L. Pessaint, A. V. Ry, K. Blade, R. Brown, A. Cook, B. Finneyfrock, A. Dodson, E. Teow, J. Velasco, R. Zahn, F. Wegmann, E. A. Bondzie, G. Dagotto, M. S. Gebre, X. He, C. Jacob-Dolan, M. Kirilova, N. Kordana, Z. Lin, L. F. Maxfield, F. Nampanya, R.

Nityanandam, J. D. Ventura, H. Wan, Y. Cai, B. Chen, A. G. Schmidt, D. R. Wesemann, R. S. Baric, G. Alter, H. Andersen, M. G. Lewis, D. H. Barouch, DNA vaccine protection against SARS-CoV-2 in rhesus macaques. *Science*. **369**, 806–811 (2020).
50. B. Isho, K. T. Abe, M. Zuo, A. J. Jamal, B. Rathod, J. H. Wang, Z. Li, G. Chao, O. L. Rojas, Y. M. Bang, A. Pu, N. Christie-Holmes, C. Gervais, D. Ceccarelli, P. Samavarchi-Tehrani, F. Guvenc, P. Budylowski, A. Li, A. Paterson, F. Y. Yue, L. M. Marin, L. Caldwell, J. L. Wrana, K. Colwill, F. Sicheri, S. Mubareka, S. D. Gray-Owen, S. J. Drews, W. L. Siqueira, M. Barrios-Rodiles, M. Ostrowski, J. M. Rini, Y. Durocher, A. J. McGeer, J. L. Gommerman, A.-C. Gingras, Persistence of serum and saliva antibody responses to SARS-CoV-2 spike antigens in COVID-19 patients. *Sci Immunol*. **5** (2020), doi:10.1126/sciimmunol.abe5511.
51. C. W. Davis, K. J. L. Jackson, A. K. McElroy, P. Halfmann, J. Huang, C. Chennareddy, A. E. Piper, Y. Leung, C. G. Albariño, I. Crozier, A. H. Ellebedy, J. Sidney, A. Sette, T. Yu, S. C. A. Nielsen, A. J. Goff, C. F. Spiropoulou, E. O. Saphire, G. Cavet, Y. Kawaoka, A. K. Mehta, P. J. Glass, S. D. Boyd, R. Ahmed, Longitudinal Analysis of the Human B Cell Response to Ebola Virus Infection. *Cell*. **177**, 1566-1582.e17 (2019).
52. A. Z. Wec, D. Haslwanter, Y. N. Abdiche, L. Shehata, N. Pedreño-Lopez, C. L. Moyer, Z. A. Bornholdt, A. Lilov, J. H. Nett, R. K. Jangra, M. Brown, D. I. Watkins, C. Ahlm, M. N. Forsell, F. A. Rey, G. Barba-Spaeth, K. Chandran, L. M. Walker, Longitudinal dynamics of the human B cell response to the yellow fever 17D vaccine. *Proc National Acad Sci*. **117**, 6675–6685 (2020).
53. J. Neidleman, X. Luo, J. Frouard, G. Xie, G. Gill, E. S. Stein, M. McGregor, T. Ma, A. F. George, A. Kosters, W. C. Greene, J. Vasquez, E. Ghosn, S. Lee, N. R. Roan, SARS-CoV-2-specific T cells exhibit phenotypic features of robust helper function, lack of terminal differentiation, and high proliferative potential. *Cell Reports Medicine*, 100081 (2020).
54. S. Sridhar, S. Begom, A. Bermingham, K. Hoschler, W. Adamson, W. Carman, T. Bean, W. Barclay, J. J. Deeks, A. Lalvani, Cellular immune correlates of protection against symptomatic pandemic influenza. *Nat Med*. **19**, 1305–1312 (2013).
55. R. S. Akondy, M. Fitch, S. Edupuganti, S. Yang, H. T. Kissick, K. W. Li, B. A. Youngblood, H. A. Abdelsamed, D. J. McGuire, K. W. Cohen, G. Alexe, S. Nagar, M. M. McCausland, S. Gupta, P. Tata, W. N. Haining, M. J. McElrath, D. Zhang, B. Hu, W. J. Greenleaf, J. J. Goronzy, M. J. Mulligan, M. Hellerstein, R. Ahmed, Origin and differentiation of human memory CD8 T cells after vaccination. *Nature*. **552**, 362–367 (2017).
56. S. Crotty, T Follicular Helper Cell Biology: A Decade of Discovery and Diseases. *Immunity*. **50**, 1132–1148 (2019).
57. J. A. Juno, H.-X. Tan, W. S. Lee, A. Reynaldi, H. G. Kelly, K. Wragg, R. Esterbauer, H. E. Kent, C. J. Batten, F. L. Mordant, N. A. Gherardin, P. Pymm, M. H. Dietrich, N. E. Scott, W.-H. Tham, D. I. Godfrey, K. Subbarao, M. P. Davenport, S. J. Kent, A. K. Wheatley, Humoral and circulating follicular helper T cell responses in recovered patients with COVID-19. *Nat Med*, 1–7 (2020).
58. S. Crotty, P. Felgner, H. Davies, J. Glidewell, L. Villarreal, R. Ahmed, Cutting Edge: Long-Term B Cell Memory in Humans after Smallpox Vaccination. *J Immunol*. **171**, 4969–4973 (2003).
59. X. Yu, T. Tsibane, P. A. McGraw, F. S. House, C. J. Keefer, M. D. Hicar, T. M. Tumpey, C. Pappas, L. A. Perrone, O. Martinez, J. Stevens, I. A. Wilson, P. V. Aguilar, E. L. Altschuler, C. F. Basler, J. E. C. Jr, Neutralizing antibodies derived from the B cells of 1918 influenza pandemic survivors. *Nature*. **455**, 532–536 (2008).
60. E. Hammarlund, M. W. Lewis, S. G. Hansen, L. I. Strelow, J. A. Nelson, G. J. Sexton, J. M. Hanifin, M. K. Slifka, Duration of antiviral immunity after smallpox vaccination. *Nature Medicine*. **9**, 1131–1137 (2003).

61. N. L. Bert, A. T. Tan, K. Kunasegaran, C. Y. L. Tham, M. Hafezi, A. Chia, M. H. Y. Chng, M. Lin, N. Tan, M. Linster, W. N. Chia, M. I.-C. Chen, L.-F. Wang, E. E. Ooi, S. Kalimuddin, P. A. Tambyah, J. G.-H. Low, Y.-J. Tan, A. Bertoletti, SARS-CoV-2-specific T cell immunity in cases of COVID-19 and SARS, and uninfected controls. *Nature*. **584**, 457–462 (2020).
62. N. B. Mercado, R. Zahn, F. Wegmann, C. Loos, A. Chandrashekar, J. Yu, J. Liu, L. Peter, K. McMahan, L. H. Tostanoski, X. He, D. R. Martinez, L. Rutten, R. Bos, D. van Manen, J. Vellinga, J. Custers, J. P. Langedijk, T. Kwaks, M. J. G. Bakkers, D. Zuijdgeest, S. K. R. Huber, C. Atyeo, S. Fischinger, J. S. Burke, J. Feldman, B. M. Hauser, T. M. Caradonna, E. A. Bondzie, G. Dagotto, M. S. Gebre, E. Hoffman, C. Jacob-Dolan, M. Kirilova, Z. Li, Z. Lin, S. H. Mahrokhian, L. F. Maxfield, F. Nampanya, R. Nityanandam, J. P. Nkolola, S. Patel, J. D. Ventura, K. Verrington, H. Wan, L. Pessaint, A. V. Ry, K. Blade, A. Strasbaugh, M. Cabus, R. Brown, A. Cook, S. Zouantchangadou, E. Teow, H. Andersen, M. G. Lewis, Y. Cai, B. Chen, A. G. Schmidt, R. K. Reeves, R. S. Baric, D. A. Lauffenburger, G. Alter, P. Stoffels, M. Mammen, J. V. Hoof, H. Schuitemaker, D. H. Barouch, Single-shot Ad26 vaccine protects against SARS-CoV-2 in rhesus macaques. *Nature*, 1–11 (2020).
63. K. S. Corbett, B. Flynn, K. E. Foulds, J. R. Francica, S. Boyoglu-Barnum, A. P. Werner, B. Flach, S. O'Connell, K. W. Bock, M. Minai, B. M. Nagata, H. Anderson, D. R. Martinez, A. T. Noe, N. Douek, M. M. Donaldson, N. N. Nji, G. S. Alvarado, D. K. Edwards, D. R. Flebbe, E. Lamb, N. A. Doria-Rose, B. C. Lin, M. K. Louder, S. O'Dell, S. D. Schmidt, E. Phung, L. A. Chang, C. Yap, J.-P. M. Todd, L. Pessaint, A. V. Ry, S. Browne, J. Greenhouse, T. Putman-Taylor, A. Strasbaugh, T.-A. Campbell, A. Cook, A. Dodson, K. Steingrebe, W. Shi, Y. Zhang, O. M. Abiona, L. Wang, A. Pegu, E. S. Yang, K. Leung, T. Zhou, I.-T. Teng, A. Widge, I. Gordon, L. Novik, R. A. Gillespie, R. J. Loomis, J. I. Moliva, G. Stewart-Jones, S. Himansu, W.-P. Kong, M. C. Nason, K. M. Morabito, T. J. Ruckwardt, J. E. Ledgerwood, M. R. Gaudinski, P. D. Kwong, J. R. Mascola, A. Carfi, M. G. Lewis, R. S. Baric, A. McDermott, I. N. Moore, N. J. Sullivan, M. Roederer, R. A. Seder, B. S. Graham, Evaluation of the mRNA-1273 Vaccine against SARS-CoV-2 in Nonhuman Primates. *New Engl J Med* (2020), doi:10.1056/nejmoa2024671.
64. L. Corey, J. R. Mascola, A. S. Fauci, F. S. Collins, A strategic approach to COVID-19 vaccine R&D. *Science*. **368**, 948–950 (2020).
65. J. Zhao, J. Zhao, A. K. Mangalam, R. Channappanavar, C. Fett, D. K. Meyerholz, S. Agnihothram, R. S. Baric, C. S. David, S. Perlman, Airway Memory CD4 + T Cells Mediate Protective Immunity against Emerging Respiratory Coronaviruses. *Immunity*. **44**, 1379–1391 (2016).
66. W. E. Purtha, T. F. Tedder, S. Johnson, D. Bhattacharya, M. S. Diamond, Memory B cells, but not long-lived plasma cells, possess antigen specificities for viral escape mutants. *The Journal of experimental medicine*. **208**, 2599–2606 (2011).
67. D. Masopust, A. G. Soerens, Tissue-Resident T Cells and Other Resident Leukocytes. *Annu Rev Immunol*. **37**, 521–546 (2019).
68. H. C. Whittle, P. Aaby, B. Samb, H. Jensen, J. Bennett, F. Simondon, Effect of subclinical infection on maintaining immunity against measles in vaccinated children in West Africa. *Lancet*. **353**, 98–102 (1999).
69. S. A. Plotkin, Vaccines: correlates of vaccine-induced immunity. *Clinical infectious diseases : an official publication of the Infectious Diseases Society of America*. **47**, 401–409 (2008).
70. N. Burdin, L. K. Handy, S. A. Plotkin, What Is Wrong with Pertussis Vaccine Immunity? The Problem of Waning Effectiveness of Pertussis Vaccines. *Cold Spring Harbor perspectives in biology*. **9**, a029454 (2017).
71. N. van Doremalen, T. Lambe, A. Spencer, S. Belij-Rammerstorfer, J. N. Purushotham, J. R. Port, V. A. Avanzato, T. Bushmaker, A. Flaxman, M. Ulaszewska, F. Feldmann, E. R. Allen, H. Sharpe, J. Schulz, M. Holbrook, A. Okumura, K. Meade-White, L. Pérez-Pérez, N. J. Edwards, D. Wright, C. Bissett, C. Gilbride, B. N. Williamson, R. Rosenke, D. Long, A. Ishwarbhai, R. Kailath, L. Rose, S. Morris, C. Powers,

J. Lovaglio, P. W. Hanley, D. Scott, G. Saturday, E. de Wit, S. C. Gilbert, V. J. Munster, ChAdOx1 nCoV-19 vaccine prevents SARS-CoV-2 pneumonia in rhesus macaques. *Nature*, 1–5 (2020).
72. R. L. Tillett, J. R. Sevinsky, P. D. Hartley, H. Kerwin, N. Crawford, A. Gorzalski, C. Laverdure, S. C. Verma, C. C. Rossetto, D. Jackson, M. J. Farrell, S. V. Hooser, M. Pandori, Genomic evidence for reinfection with SARS-CoV-2: a case study. *Lancet Infect Dis* (2020), doi:10.1016/s1473-3099(20)30764-7.
73. K. K.-W. To, I. F.-N. Hung, J. D. Ip, A. W.-H. Chu, W.-M. Chan, A. R. Tam, C. H.-Y. Fong, S. Yuan, H.-W. Tsoi, A. C.-K. Ng, L. L.-Y. Lee, P. Wan, E. Y.-K. Tso, W.-K. To, D. N.-C. Tsang, K.-H. Chan, J.-D. Huang, K.-H. Kok, V. C.-C. Cheng, K.-Y. Yuen, COVID-19 re-infection by a phylogenetically distinct SARS-coronavirus-2 strain confirmed by whole genome sequencing. *Clin Infect Dis* (2020), doi:10.1093/cid/ciaa1275.
74. J. H. Beigel, K. M. Tomashek, L. E. Dodd, A. K. Mehta, B. S. Zingman, A. C. Kalil, E. Hohmann, H. Y. Chu, A. Luetkemeyer, S. Kline, D. L. de Castilla, R. W. Finberg, K. Dierberg, V. Tapson, L. Hsieh, T. F. Patterson, R. Paredes, D. A. Sweeney, W. R. Short, G. Touloumi, D. C. Lye, N. Ohmagari, M.-D. Oh, G. M. Ruiz-Palacios, T. Benfield, G. Fätkenheuer, M. G. Kortepeter, R. L. Atmar, C. B. Creech, J. Lundgren, A. G. Babiker, S. Pett, J. D. Neaton, T. H. Burgess, T. Bonnett, M. Green, M. Makowski, A. Osinusi, S. Nayak, H. C. Lane, A.-1 S. G. Members, Remdesivir for the Treatment of Covid-19 — Final Report. *New Engl J Med* (2020), doi:10.1056/nejmoa2007764.
75. F. Amanat, D. Stadlbauer, S. Strohmeier, T. H. O. Nguyen, V. Chromikova, M. McMahon, K. Jiang, G. A. Arunkumar, D. Jurczyszak, J. Polanco, M. Bermudez-Gonzalez, G. Kleiner, T. Aydillo, L. Miorin, D. S. Fierer, L. A. Lugo, E. M. Kojic, J. Stoever, S. T. H. Liu, C. Cunningham-Rundles, P. L. Felgner, T. Moran, A. García-Sastre, D. Caplivski, A. C. Cheng, K. Kedzierska, O. Vapalahti, J. M. Hepojoki, V. Simon, F. Krammer, A serological assay to detect SARS-CoV-2 seroconversion in humans. *Nat Med*. **26**, 1033–1036 (2020).
76. J. Mestecky, R. G. Hamilton, C. G. M. Magnusson, R. Jefferis, J. P. Vaerman, M. Goodall, G. G. de Lange, I. Moro, P. Aucouturier, J. Radl, C. Cambiaso, C. Silvain, J. L. Preud'homme, K. Kusama, G. M. Carlone, J. Biewenga, K. Kobayashi, F. Skvaril, C. B. Reimer, Evaluation of monoclonal antibodies with specificity for human IgA, IgA subclasses and allotypes and secretory component Results of an IUIS/WHO collaborative study. *J Immunol Methods*. **193**, 103–148 (1996).
77. GraphPad, GraphPad Prism 8 Curve Fitting Guide (2020), (available at https://www.graphpad.com/guides/prism/8/curve-fitting/index.htm).

Figure 1

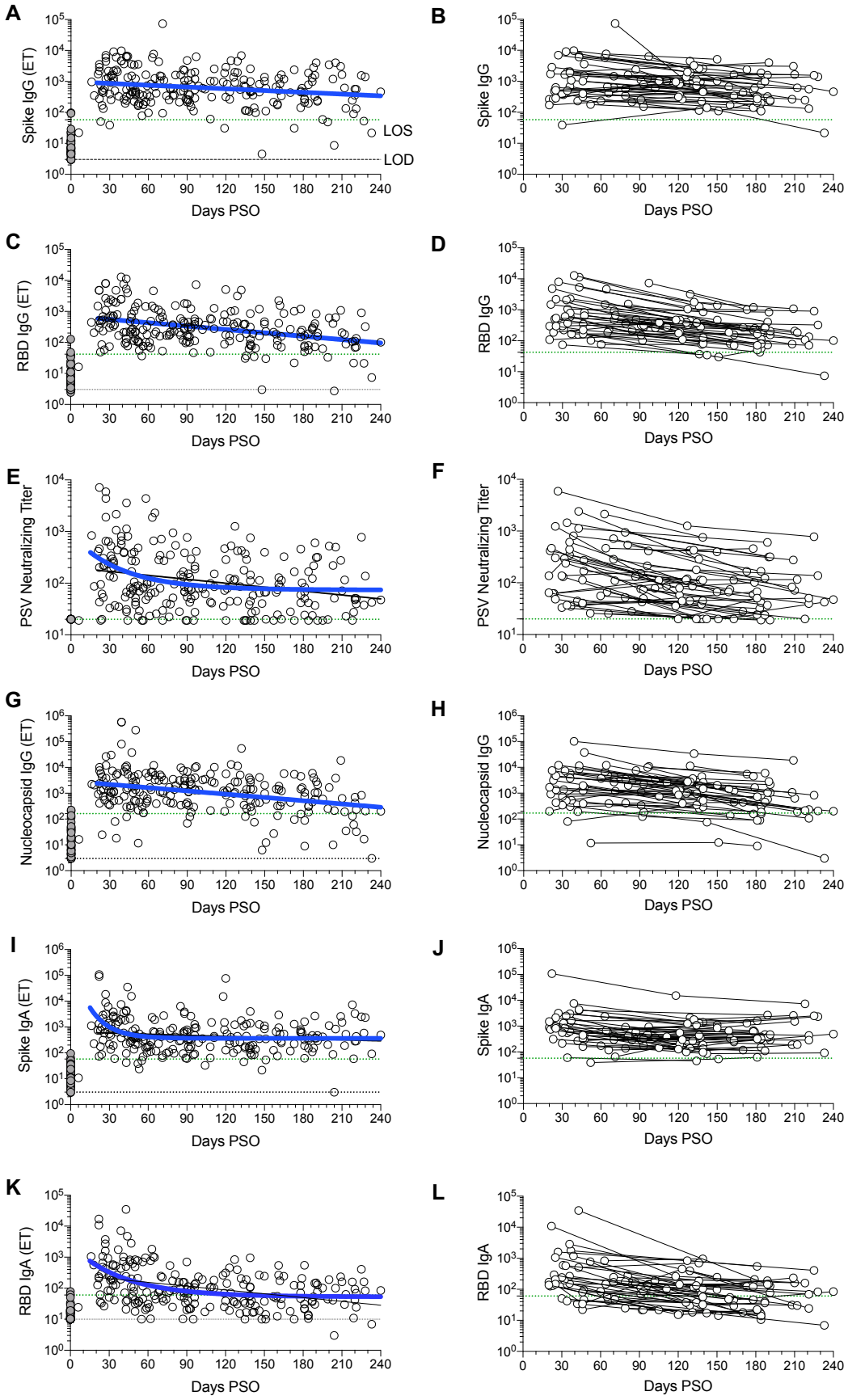
A
Spike IgG (ET)
LOS
LOD
Days PSO
B
Spike IgG
Days PSO
C
RBD IgG (ET)
Days PSO
D
RBD IgG
Days PSO
E
PSV Neutralizing Titer
Days PSO
F
PSV Neutralizing Titer
Days PSO
G
Nucleocapsid IgG (ET)
Days PSO
H
Nucleocapsid IgG
Days PSO
I
Spike IgA (ET)
Days PSO
J
Spike IgA
Days PSO
K
RBD IgA (ET)
Days PSO
L
RBD IgA
Days PSO

Figure 2

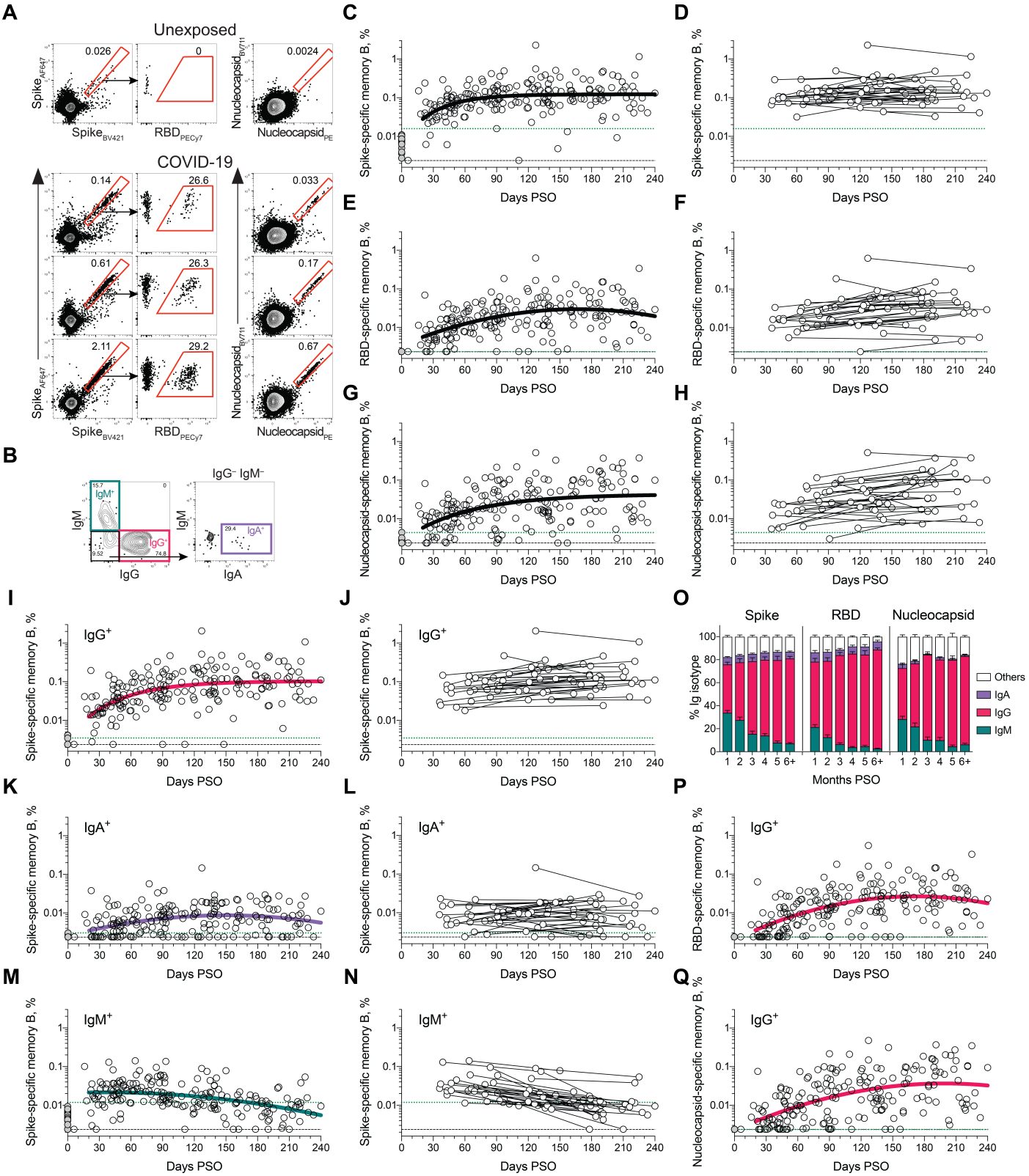
A
Unexposed
COVID-19
Spike
RBD
Nucleocapsid
B
IgG⁻ IgM⁻
IgM
IgG
IgA
C
D
E
F
G
H
I
J
K
L
M
N
O
P
Q
Spike-specific memory B, %
RBD-specific memory B, %
Nucleocapsid-specific memory B, %
Days PSO
IgG⁺
IgA⁺
IgM⁺
% Ig isotype
Months PSO
Others
IgA
IgG
IgM

Figure 3

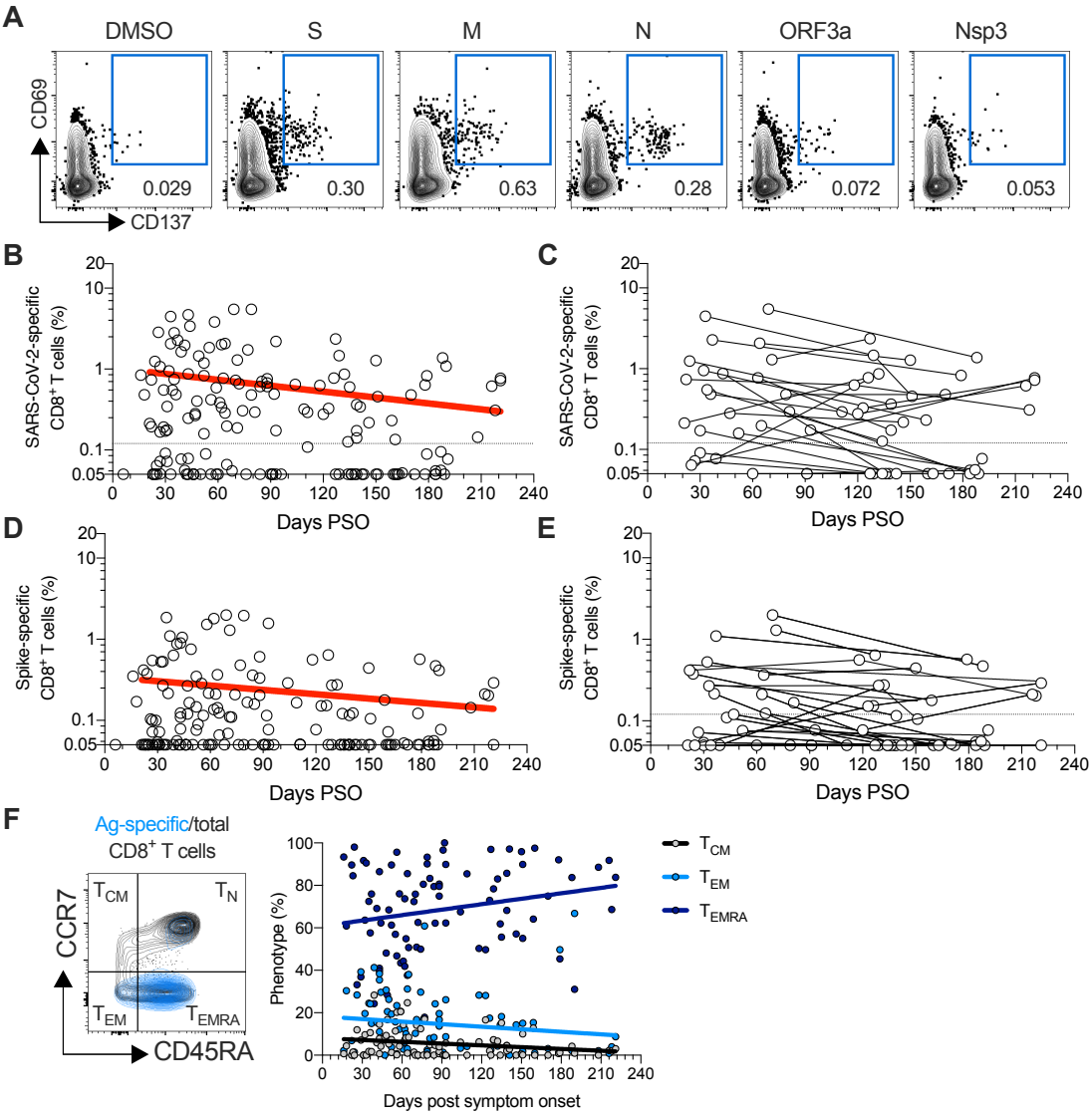
A
DMSO
S
M
N
ORF3a
Nsp3
CD69
CD137
0.029
0.30
0.63
0.28
0.072
0.053
B
SARS-CoV-2-specific CD8+ T cells (%)
Days PSO
C
SARS-CoV-2-specific CD8+ T cells (%)
Days PSO
D
Spike-specific CD8+ T cells (%)
Days PSO
E
Spike-specific CD8+ T cells (%)
Days PSO
F
Ag-specific/total CD8+ T cells
CCR7
CD45RA
TCM
TN
TEM
TEMRA
Phenotype (%)
Days post symptom onset
TCM
TEM
TEMRA

Figure 4

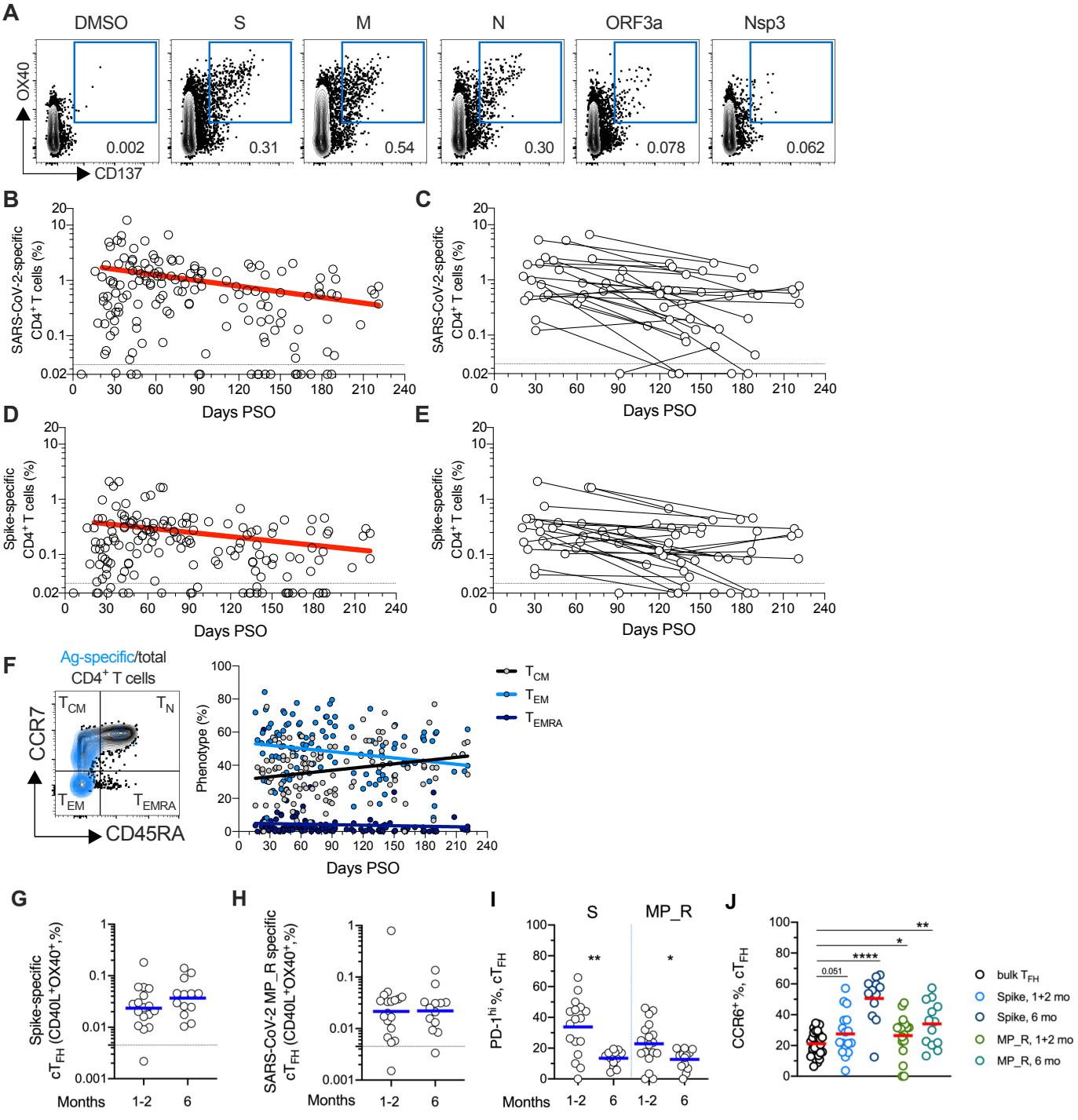
A
DMSO
S
M
N
ORF3a
Nsp3
OX40
CD137
0.002
0.31
0.54
0.30
0.078
0.062
B
SARS-CoV-2-specific CD4+ T cells (%)
Days PSO
C
SARS-CoV-2-specific CD4+ T cells (%)
Days PSO
D
Spike-specific CD4+ T cells (%)
Days PSO
E
Spike-specific CD4+ T cells (%)
Days PSO
F
Ag-specific/total CD4+ T cells
CCR7
CD45RA
TCM
TN
TEM
TEMRA
Phenotype (%)
Days PSO
TCM
TEM
TEMRA
G
Spike-specific cTFH (CD40L+OX40+,%)
Months
1-2
6
H
SARS-CoV-2 MP_R specific cTFH (CD40L+OX40+,%)
Months
1-2
6
I
S
MP_R
PD-1hi %, cTFH
Months
1-2
6
1-2
6
J
CCR6+ %, cTFH
0.051
bulk TFH
Spike, 1+2 mo
Spike, 6 mo
MP_R, 1+2 mo
MP_R, 6 mo

Figure 5

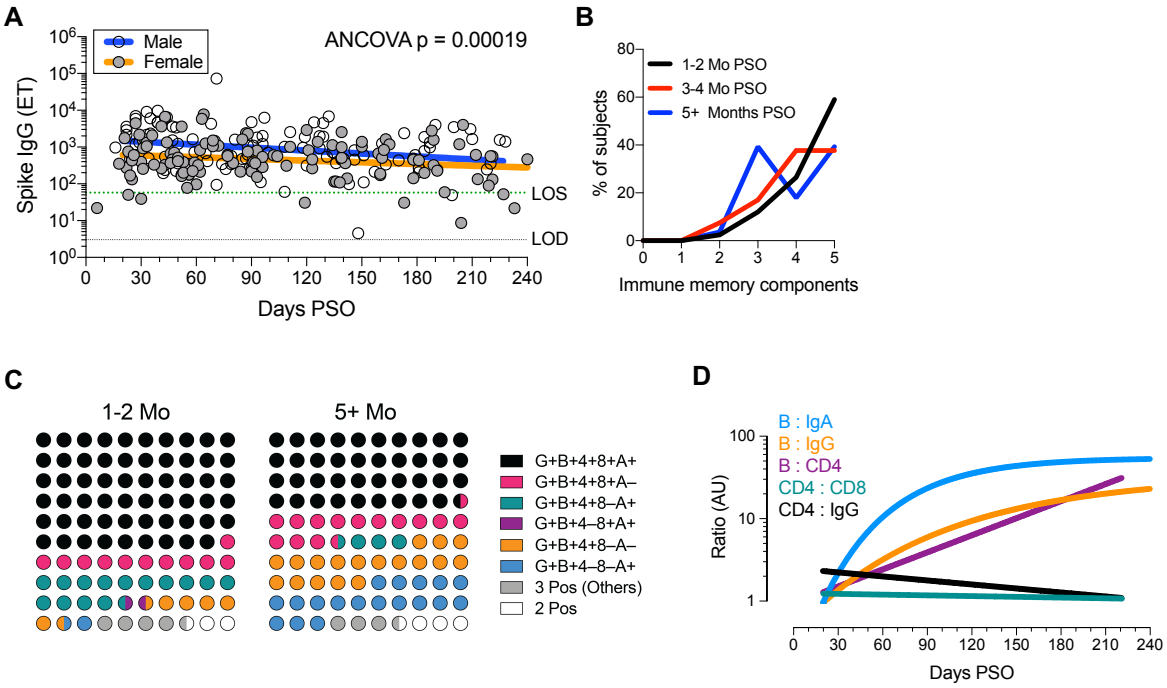
A
Male
Female
ANCOVA p = 0.00019
Spike IgG (ET)
LOS
LOD
Days PSO
B
1-2 Mo PSO
3-4 Mo PSO
5+ Months PSO
% of subjects
Immune memory components
C
1-2 Mo
5+ Mo
G+B+4+8+A+
G+B+4+8+A–
G+B+4+8–A+
G+B+4–8+A+
G+B+4+8–A–
G+B+4–8–A+
3 Pos (Others)
2 Pos
D
B : IgA
B : IgG
B : CD4
CD4 : CD8
CD4 : IgG
Ratio (AU)
Days PSO

Figure S1

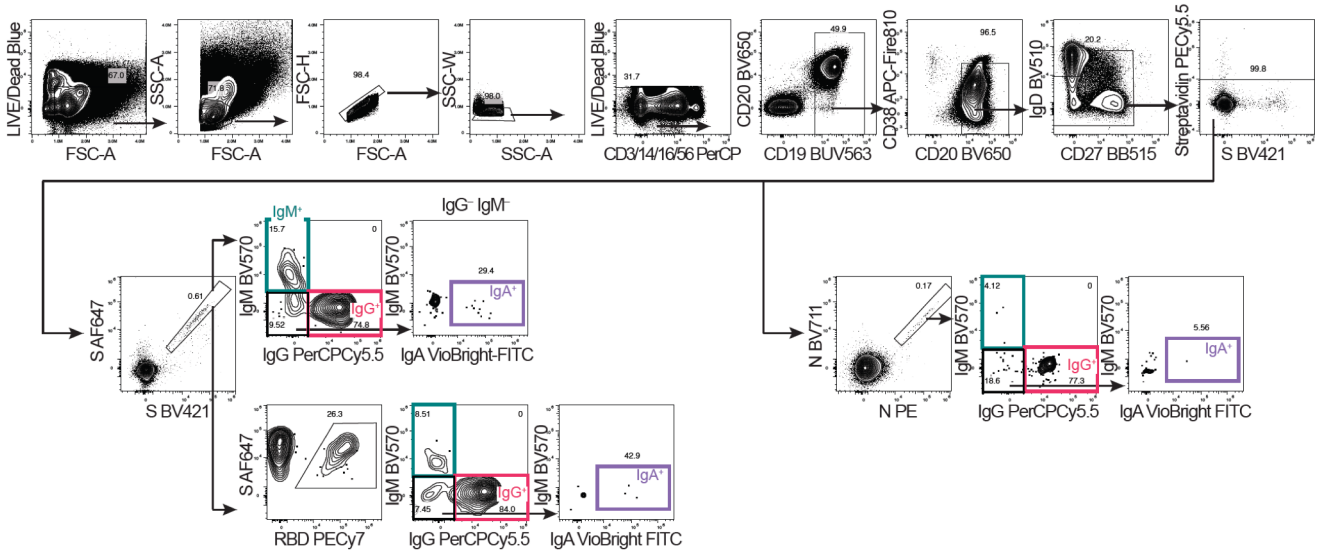
LIVE/Dead Blue
FSC-A
SSC-A
FSC-H
SSC-W
CD3/14/16/56 PerCP
CD20 BV650
CD19 BUV563
CD38 APC-Fire810
CD27 BB515
IgD BV510
Streptavidin PECy5.5
S BV421
S AF647
IgM BV570
IgG PerCPCy5.5
IgA VioBright-FITC
IgG⁻ IgM⁻
IgM⁺
IgG⁺
IgA⁺
RBD PECy7
N BV711
N PE
IgA VioBright FITC

Figure S2

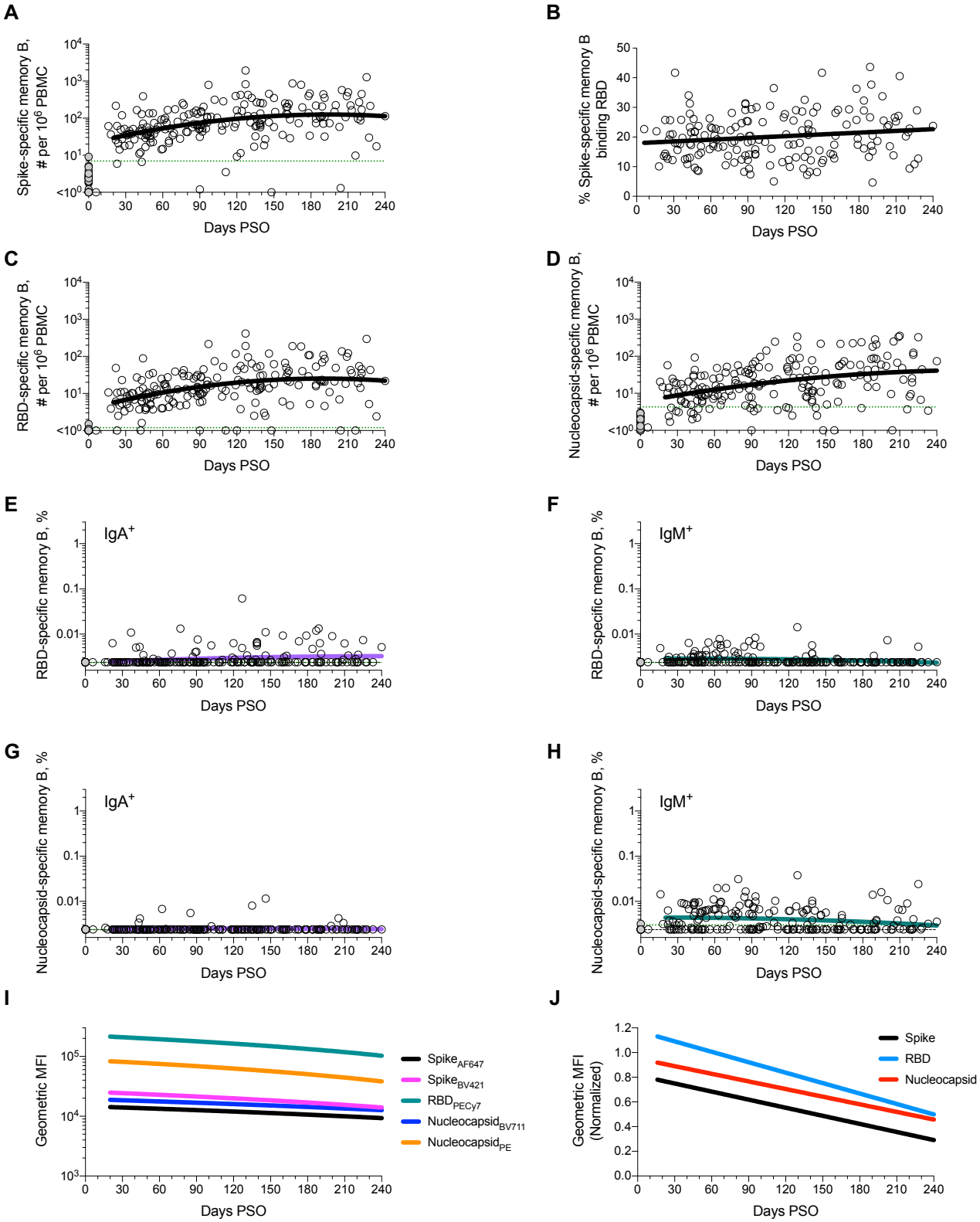
A
Spike-specific memory B, # per 10^6 PBMC
Days PSO
B
% Spike-specific memory B binding RBD
Days PSO
C
RBD-specific memory B, # per 10^6 PBMC
Days PSO
D
Nucleocapsid-specific memory B, # per 10^6 PBMC
Days PSO
E
IgA+
RBD-specific memory B, %
Days PSO
F
IgM+
RBD-specific memory B, %
Days PSO
G
IgA+
Nucleocapsid-specific memory B, %
Days PSO
H
IgM+
Nucleocapsid-specific memory B, %
Days PSO
I
Geometric MFI
Days PSO
Spike AF647
Spike BV421
RBD PECy7
Nucleocapsid BV711
Nucleocapsid PE
J
Geometric MFI (Normalized)
Days PSO
Spike
RBD
Nucleocapsid

Figure S3

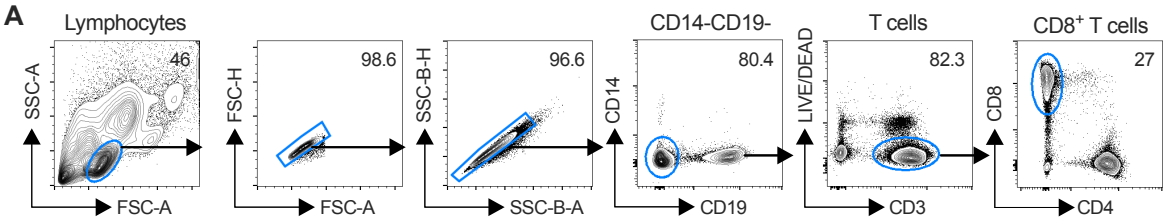
A
Lymphocytes
SSC-A
FSC-A
46
FSC-H
FSC-A
98.6
SSC-B-H
SSC-B-A
96.6
CD14-CD19-
CD14
CD19
80.4
T cells
LIVE/DEAD
CD3
82.3
CD8+ T cells
CD8
CD4
27

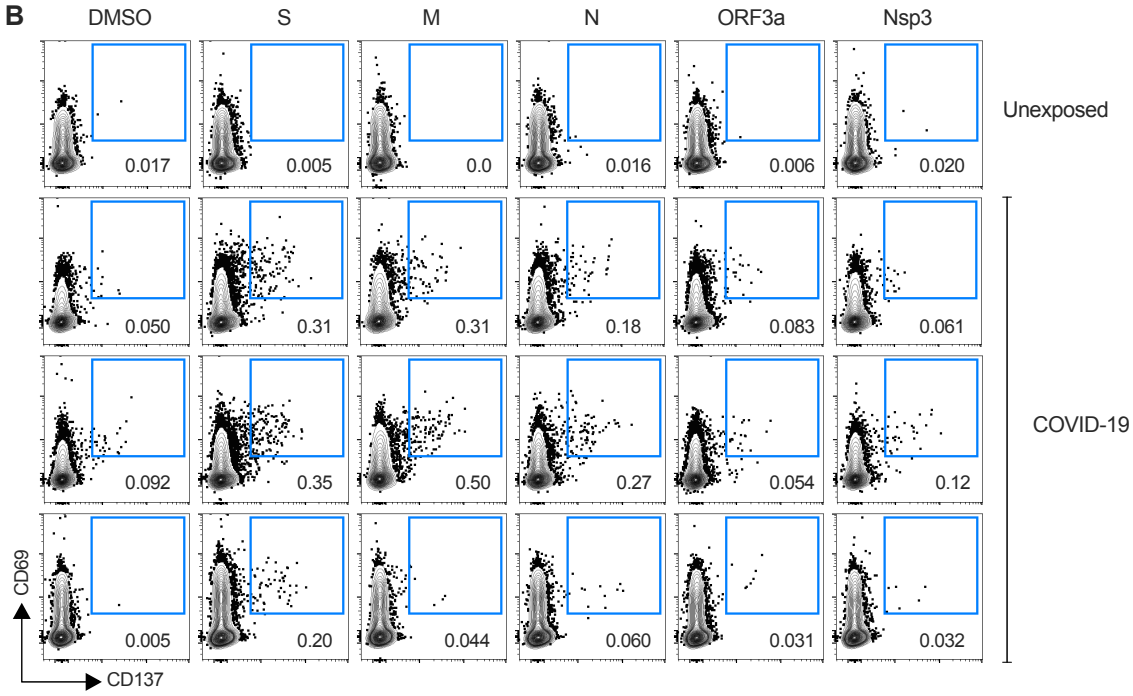
B
DMSO
S
M
N
ORF3a
Nsp3
Unexposed
COVID-19
0.017
0.005
0.0
0.016
0.006
0.020
0.050
0.31
0.31
0.18
0.083
0.061
0.092
0.35
0.50
0.27
0.054
0.12
0.005
0.20
0.044
0.060
0.031
0.032
CD69
CD137

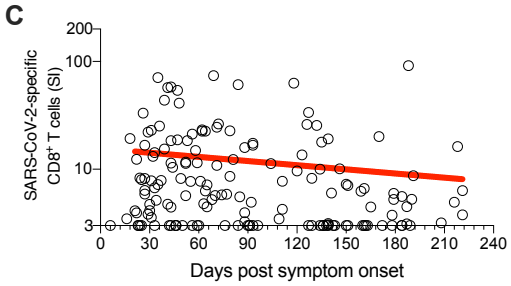
C
SARS-CoV-2-specific CD8+ T cells (SI)
200
100
10
3
0
30
60
90
120
150
180
210
240
Days post symptom onset

Figure S4

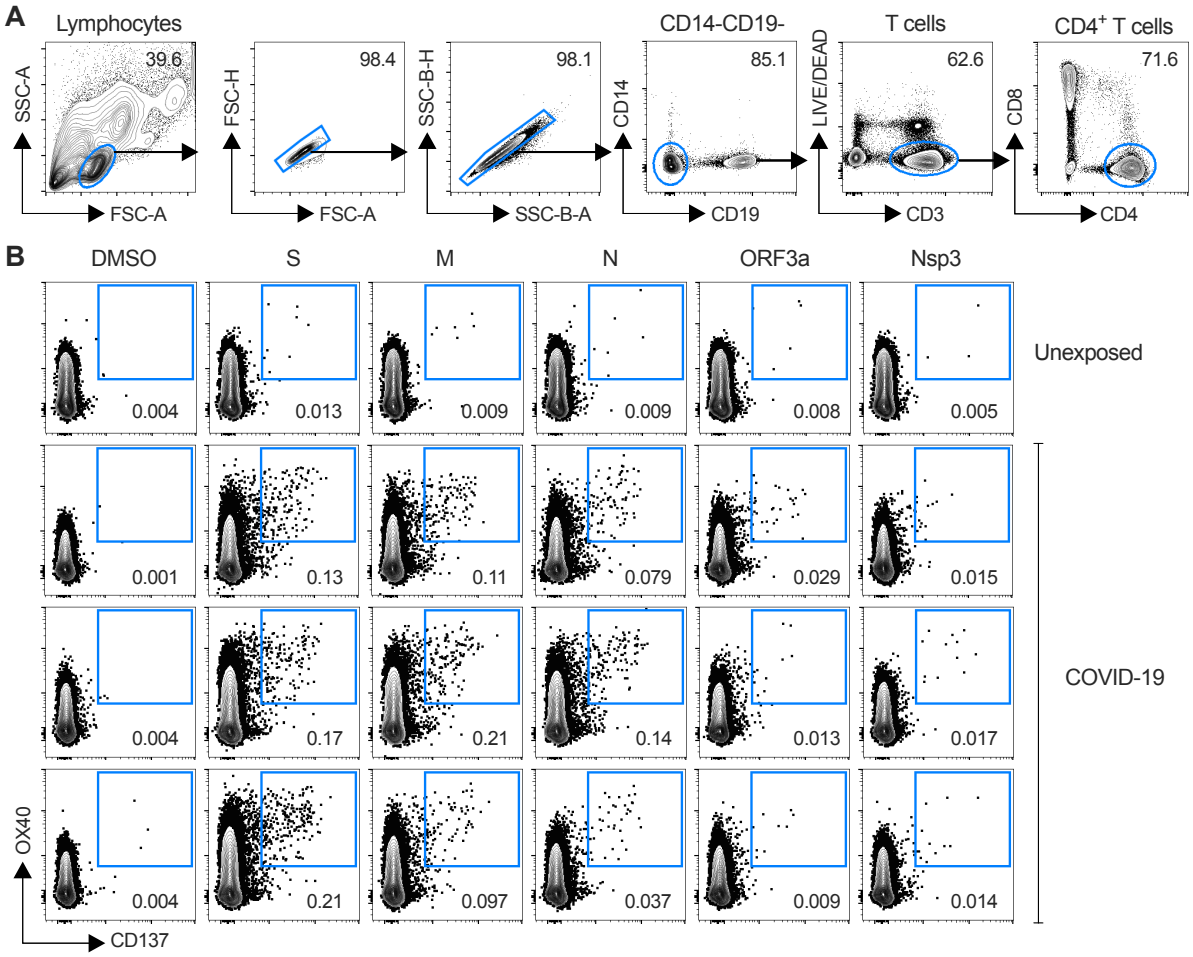
A
Lymphocytes
39.6
SSC-A
FSC-A
98.4
FSC-H
FSC-A
98.1
SSC-B-H
SSC-B-A
CD14-CD19-
85.1
CD14
CD19
T cells
62.6
LIVE/DEAD
CD3
CD4+ T cells
71.6
CD8
CD4
B
DMSO
S
M
N
ORF3a
Nsp3
Unexposed
0.004
0.013
0.009
0.009
0.008
0.005
COVID-19
0.001
0.13
0.11
0.079
0.029
0.015
0.004
0.17
0.21
0.14
0.013
0.017
0.004
0.21
0.097
0.037
0.009
0.014
OX40
CD137

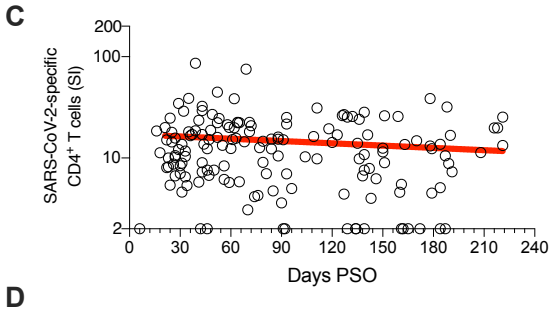
C
SARS-CoV-2-specific CD4+ T cells (SI)
200
100
10
2
0
30
60
90
120
150
180
210
240
Days PSO

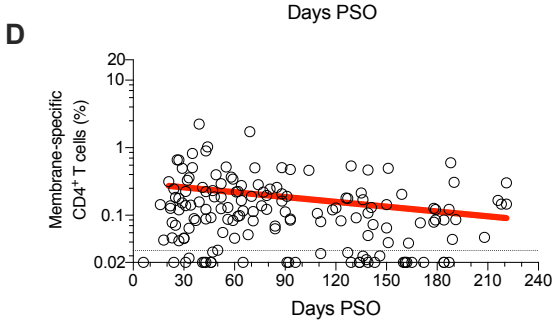
D
Membrane-specific CD4+ T cells (%)
20
10
1
0.1
0.02
0
30
60
90
120
150
180
210
240
Days PSO

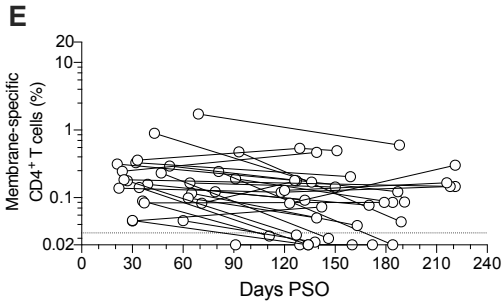
E
Membrane-specific CD4+ T cells (%)
20
10
1
0.1
0.02
0
30
60
90
120
150
180
210
240
Days PSO

Figure S5

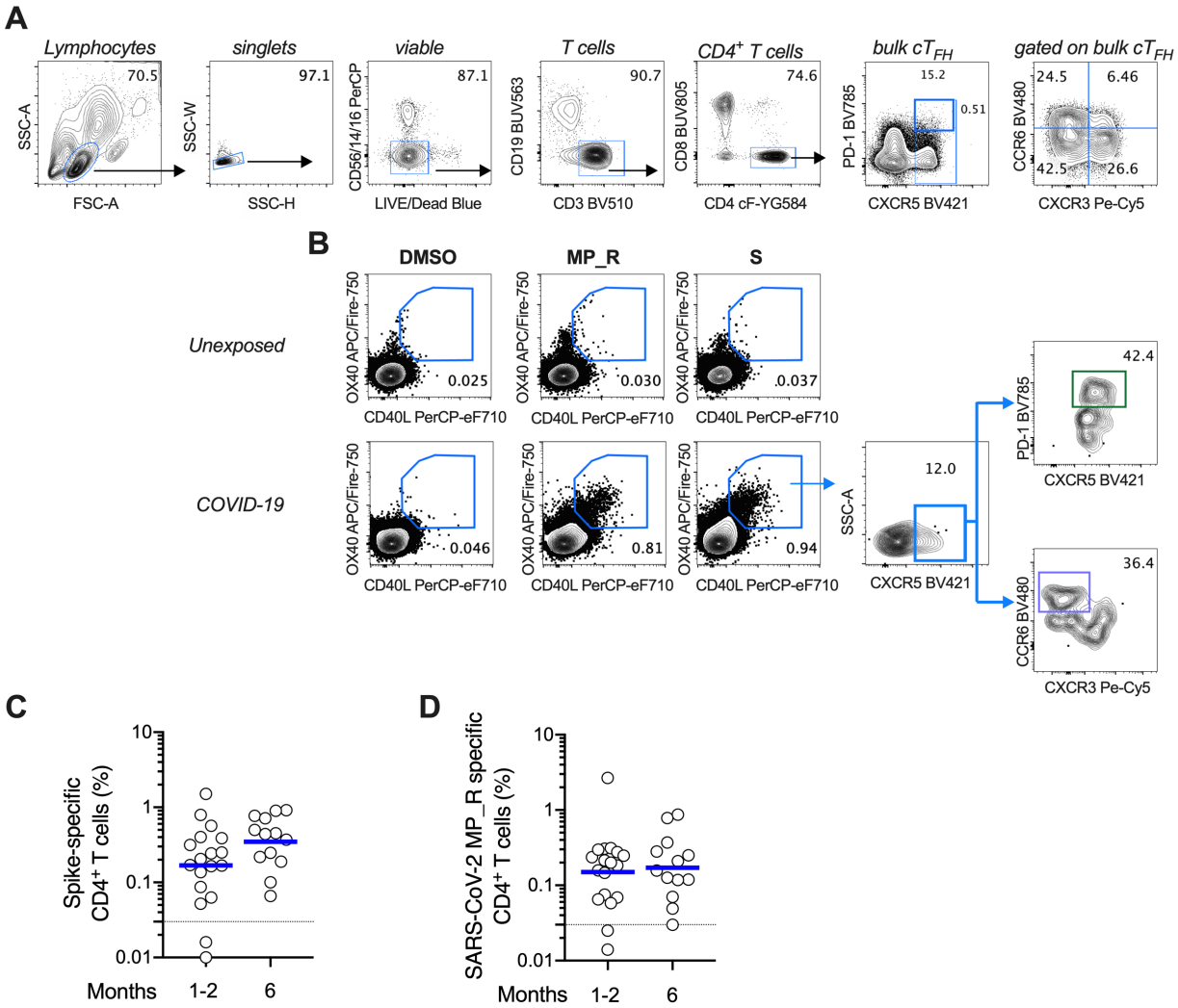
A
Lymphocytes
70.5
SSC-A
FSC-A
singlets
97.1
SSC-W
SSC-H
viable
87.1
CD56/14/16 PerCP
LIVE/Dead Blue
T cells
90.7
CD19 BUV563
CD3 BV510
CD4+ T cells
74.6
CD8 BUV805
CD4 cF-YG584
bulk cTFH
15.2
0.51
PD-1 BV785
CXCR5 BV421
gated on bulk cTFH
24.5
6.46
42.5
26.6
CCR6 BV480
CXCR3 Pe-Cy5
B
DMSO
MP_R
S
Unexposed
COVID-19
OX40 APC/Fire-750
CD40L PerCP-eF710
0.025
0.030
0.037
0.046
0.81
0.94
12.0
SSC-A
CXCR5 BV421
42.4
PD-1 BV785
36.4
CCR6 BV480
CXCR3 Pe-Cy5
C
Spike-specific CD4+ T cells (%)
10
1
0.1
0.01
Months
1-2
6
D
SARS-CoV-2 MP_R specific CD4+ T cells (%)
10
1
0.1
0.01
Months
1-2
6

Figure S6

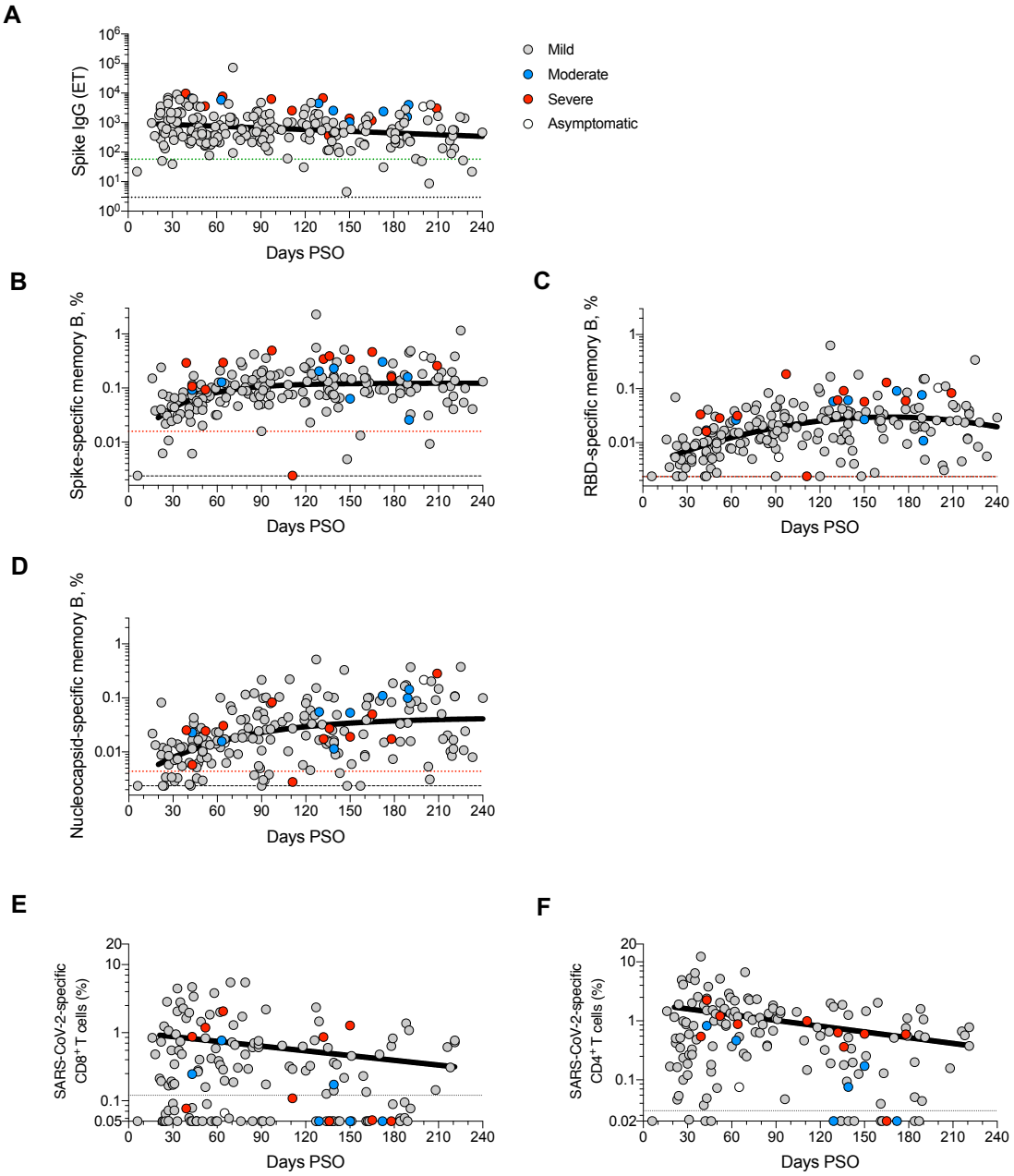
A
Spike IgG (ET)
Days PSO
Mild
Moderate
Severe
Asymptomatic
B
Spike-specific memory B, %
Days PSO
C
RBD-specific memory B, %
Days PSO
D
Nucleocapsid-specific memory B, %
Days PSO
E
SARS-CoV-2-specific CD8+ T cells (%)
Days PSO
F
SARS-CoV-2-specific CD4+ T cells (%)
Days PSO

Figure S7

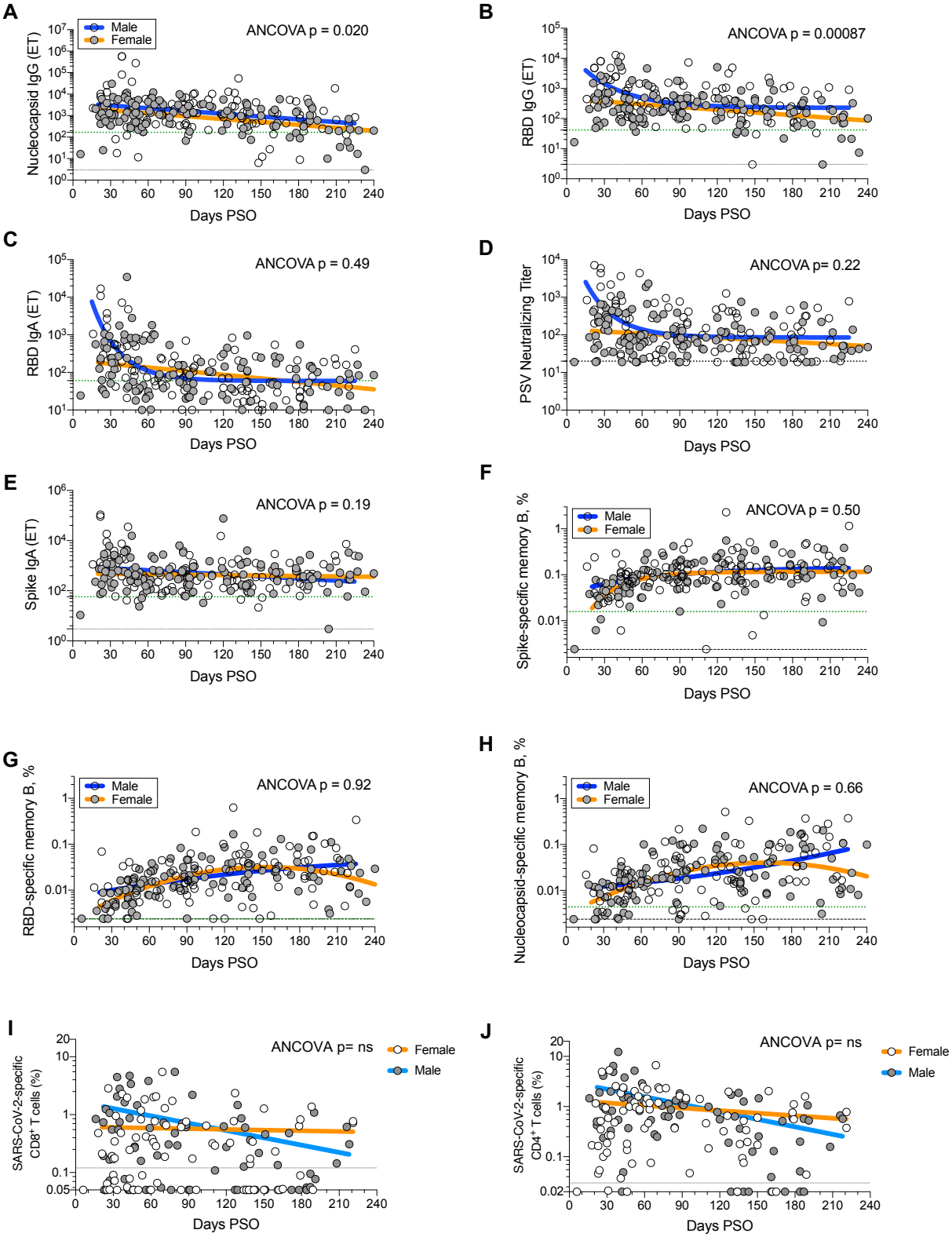
A
Male
Female
ANCOVA p = 0.020
Nucleocapsid IgG (ET)
Days PSO
B
ANCOVA p = 0.00087
RBD IgG (ET)
Days PSO
C
ANCOVA p = 0.49
RBD IgA (ET)
Days PSO
D
ANCOVA p= 0.22
PSV Neutralizing Titer
Days PSO
E
ANCOVA p = 0.19
Spike IgA (ET)
Days PSO
F
Male
Female
ANCOVA p = 0.50
Spike-specific memory B, %
Days PSO
G
Male
Female
ANCOVA p = 0.92
RBD-specific memory B, %
Days PSO
H
Male
Female
ANCOVA p = 0.66
Nucleocapsid-specific memory B, %
Days PSO
I
ANCOVA p= ns
Female
Male
SARS-CoV-2-specific CD8+ T cells (%)
Days PSO
J
ANCOVA p= ns
Female
Male
SARS-CoV-2-specific CD4+ T cells (%)
Days PSO

Figure S8

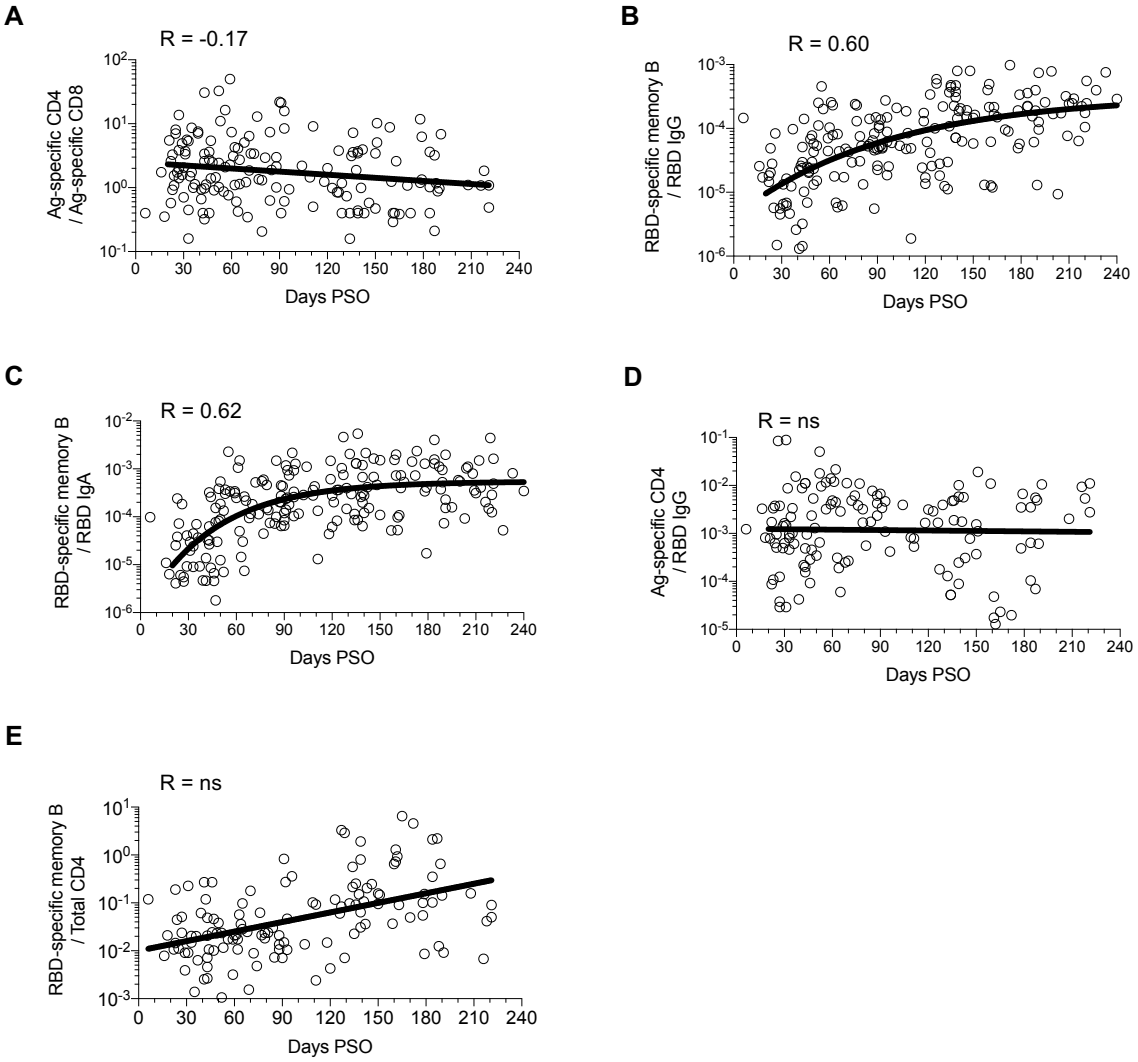
A
R = -0.17
Ag-specific CD4 / Ag-specific CD8
Days PSO
B
R = 0.60
RBD-specific memory B / RBD IgG
Days PSO
C
R = 0.62
RBD-specific memory B / RBD IgA
Days PSO
D
R = ns
Ag-specific CD4 / RBD IgG
Days PSO
E
R = ns
RBD-specific memory B / Total CD4
Days PSO